

การตรวจหารอยแตกบนภาพผิวทางแอสฟัลติกคอนกรีต โดยการวิเคราะห์กริดเซลล์แบบคัดแปร



นางสาวศิวพร ศรีเจริญ

วิทยานิพนธ์นี้เป็นส่วนหนึ่งของการศึกษาตามหลักสูตรปริญญาวิศวกรรมศาสตรมหาบัณฑิต

สาขาวิชาวิศวกรรมคอมพิวเตอร์      ภาควิชาวิศวกรรมคอมพิวเตอร์

คณะวิศวกรรมศาสตร์ จุฬาลงกรณ์มหาวิทยาลัย

ปีการศึกษา 2550

ลิขสิทธิ์ของจุฬาลงกรณ์มหาวิทยาลัย

จุฬาลงกรณ์มหาวิทยาลัย

CRACK DETECTION ON ASPHALTIC CONCRETE ROAD SURFACE IMAGES  
USING MODIFIED GRID CELL ANALYSIS



Miss Siwaporn Sorncharean

A Thesis Submitted in Partial Fulfillment of the Requirements  
for the Degree of Master of Engineering Program in Computer Engineering  
Department of Computer Engineering

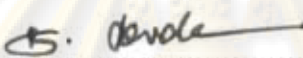
Faculty of Engineering  
Chulalongkorn University  
Academic Year 2007

Copyright of Chulalongkorn University

Thesis Title CRACK DETECTION ON ASPHALTIC CONCRETE ROAD  
SURFACE IMAGES USING MODIFIED GRID CELL ANALYSIS  
By Miss Siwaporn Sorncharean  
Field of Study Computer Engineering  
Thesis Principal Advisor Suebskul Phiphobmongkol, Ph.D.

---


Accepted by the Faculty of Engineering, Chulalongkorn University in Partial  
Fulfillment of the Requirements for the Master's Degree

  
..... Dean of the Faculty of Engineering  
(Associate Professor Boonsom Lerdhirunwong, Dr. Ing.)


THESIS COMMITTEE

  
..... Chairperson  
(Assistant Professor Wiwat Vatanawood, Ph.D.)

  
..... Thesis Principal Advisor  
(Assistant Professor Suebskul Phiphobmongkol, Ph.D.)

  
..... External Member  
(Assistant Professor Kunawee Kanitpong, Ph.D.)

  
..... Member  
(Assistant Professor Nongluk Covavisaruch)

  
..... Member  
(Associate Professor Wisanu Subsompon, Ph.D.)

ศิวพร ศรเจริญ: การตรวจหารอยแตกบนภาพผิวทางแอสฟัลติกคอนกรีตโดยการวิเคราะห์กริดเซลล์แบบดัดแปร. (CRACK DETECTION ON ASPHALTIC CONCRETE ROAD SURFACE IMAGES USING MODIFIED GRID CELL ANALYSIS)  
 อ. ที่ปรึกษาวิทยานิพนธ์หลัก: ผศ. ดร. สืบสกุล พิภพมงคล, 76 หน้า.

งานวิจัยนี้นำเสนอขั้นตอนวิธีการประมวลผลภาพบนพื้นฐานการวิเคราะห์กริดเซลล์แบบดัดแปรสำหรับการตรวจหารอยแตกบนภาพผิวทางแอสฟัลติกคอนกรีต งานวิจัยนี้มุ่งเน้นไปที่การตรวจหารอยแตกบนภาพจากกล้องถ่ายภาพแบบพื้นที่ซึ่งมักจะมีแสงไม่สม่ำเสมอเสมือนอีกทั้งการจัดการกับปัญหาของภาพที่มีพื้นผิวหยาบของแอสฟัลติกคอนกรีต

ขั้นตอนวิธีที่ใช้ในงานวิจัยนี้ ใช้การวิเคราะห์กริดเซลล์แบบดัดแปรเพื่อที่จะสกัดรอยแตกออกจากภาพ จากนั้นใช้คุณลักษณะของแรงดึงคู่ระหว่างมวลเพื่อใช้ในการกำจัดสัญญาณรบกวน และใช้เทคนิคคอนเวกซ์ฮัลล์ในการหาคุณสมบัติต่าง ๆ ของรอยแตก แล้วจึงนำคุณสมบัติเหล่านี้ไปใช้ในการแยกประเภทของรอยแตก

ความถูกต้องของขั้นตอนวิธีที่นำเสนอนี้วัด โดยการทดสอบขั้นตอนวิธีที่นำเสนอกับภาพผิวทางตามขอบข่ายของงานวิจัยซึ่งมีแสงไม่สม่ำเสมอและมีพื้นผิวหยาบ จากผลการทดสอบขั้นตอนวิธีที่นำเสนอให้ค่าความผิดพลาดเชิงบวกร้อยละ 3.07 และค่าความผิดพลาดเชิงลบร้อยละ 9.17.

นอกจากนี้งานวิจัยนี้ได้ถูกนำมาทดสอบกับภาพผิวทางที่ได้มาจากการสำรวจในสภาวะแวดล้อมเปิด ภาพผิวทางเหล่านี้ถูกนำมาตัดส่วนที่ไม่อยู่ในขอบข่ายของงานวิจัยออก ซึ่งส่วนใหญ่เป็นภาพเปียกและภาพที่ค่อนข้างมืด การทดลองนี้ให้ค่าความผิดพลาดเชิงบวกร้อยละ 6.20 และค่าความผิดพลาดเชิงลบร้อยละ 14.86

ภาควิชา วิศวกรรมคอมพิวเตอร์ ลายมือชื่อนิสิต.....ศิวพร ศรเจริญ.....  
 สาขาวิชา วิศวกรรมคอมพิวเตอร์ ลายมือชื่ออาจารย์ที่ปรึกษาวิทยานิพนธ์หลัก.....ศิวพร.....  
 ปีการศึกษา 2550

## 4970606821 : MAJOR COMPUTER ENGINEERING

KEY WORD: CRACK DETECTION / ASPHALTIC CONCRETE ROAD SURFACE / GRID CELL ANALYSIS

SIWAPORN SORNCHAREAN: CRACK DETECTION ON ASPHALTIC CONCRETE  
ROAD SURFACE IMAGES USING MODIFIED GRID CELL ANALYSIS.

THESIS PRINCIPAL ADVISOR: ASSISTANT PROFESSOR SUEBSKUL  
PHIPHOBMONGKOL, PH.D., 76 pp.

This research presents an image processing algorithm based on grid cell analysis for crack detection on asphaltic concrete road surface images. The research focuses on using pavement images from an area scan camera where light condition tend to be non-uniform and handling problems of strong texture of asphaltic concrete surface.

The algorithm uses enhanced grid cell analysis to extract crack lines from images. Then, gravitational force feature is applied to remove noise. Finally, crack objects are merged using convex hull technique to find crack characteristics which are later used to classify crack types.

The accuracy of the proposed method was measured by testing the algorithm with pavement images according to the research scope. The accuracy in finding cracked lines on pavement images with non-uniform illumination and strong texture could be achieved with an average value of 3.07% false positive and 9.17% false negative.

Moreover, the test of the proposed method in real situation was done on pavement images from the open environment survey. The dataset was manually screened so that wet pavement images and underexposed images were excluded. The dataset was then processed, resulting in 6.2% false positive and 14.86% false negative respectively.

Department: Computer Engineering Student's signature..... 

Field of study: Computer Engineering Principal advisor's signature..... 

Academic year: 2007



## Acknowledgements

This work would not have been possible without the support and encouragement of my advisor, Asst. Prof. Dr. Suebskul Phiphobmongkol. His enthusiasm, his inspiration, and his great efforts help me in numerous ways. Throughout my thesis-writing period, he provided encouragement, sound advice, good teaching, good company, and lots of good ideas. I would have been lost without him.

I would like to thank my thesis committee members, Asst. Prof. Dr. Wiwat Vatanawood, Asst. Prof. Nongluk Covavisaruch, Assoc. Prof. Dr. Wisanu Subsompon, and Asst. Prof. Dr. Kunnawee Kanitpong, for comments, recommendations and suggestions which help develop this thesis.

I am indebted to members at CGCI laboratory, Chulalongkorn University, for providing a stimulating and fun environment and to members at Transportation Institute, Chulalongkorn University, for advices and helps. I am especially grateful to Vorapong Tantisiroj and Egachai Wittayathawornwong who patiently assist me in many different ways. Weerachai Wongweeranimit, Peraluck Maneenart, and Narin Srikaew were particularly helpful in providing useful data and special mention.

I wish to acknowledge the financial support provided by Commission on Higher Education, Ministry of Education, Kingdom of Thailand, and would like to thank Department of Highways and Department of Rural Roads, Ministry of Transport, Kingdom of Thailand, for comments, recommendations and providing pavement image and road database.

I cannot end without thanking my family, on whose constant encouragement and love I have relied throughout my time at the Academy.

ศูนย์วิทยุทรัพยากร  
จุฬาลงกรณ์มหาวิทยาลัย

## Contents

	Page
Abstract (Thai) .....	iv
Abstract (English) .....	v
Acknowledgements .....	vi
Contents.....	vii
List of Tables.....	x
List of Figures .....	xi
List of Figures .....	xi
CHAPTER I INTRODUCTION .....	1
1.1 Crack Detection Difficulties .....	2
1.2 Objective .....	3
1.3 Scope of Work.....	3
1.4 Workflow .....	4
CHAPTER II LITERATURE SURVEY AND THEORY STATEMENTS .....	5
2.1 Literature Survey .....	5
2.2 Morphological Image Processing in Grayscale Image .....	6
2.2.1 Dilation and Erosion Operations .....	7
2.2.2 Opening and Closing Operations .....	8
2.3 Grid Cell Analysis (GCA) .....	10
2.4 Hill Climbing Algorithm .....	11
2.5 Law of Gravities .....	12
CHAPTER III RESEARCH METHODOLOGIES .....	13
3.1 Grid Cell Size .....	14
3.2 Pre-processing Phase.....	14
3.3 Crack Segmentation Phase .....	16
3.3.1 Grid Cell Analysis Chain.....	17
3.3.2 Crack Cell Verification .....	18
3.4 Noise Removal Phase .....	20
3.4.1 Crack Appearance .....	21

	Page
3.4.2 Gravitation Feature .....	21
3.5 Crack Identification Phase .....	23
3.5.1 Merging Method .....	24
3.5.2 Geometric Characteristics .....	26
CHAPTER IV EXPERIMENTS AND EXPERIMENTAL RESULTS .....	27
4.1 Data Resource / Data Collection .....	27
4.2 CU Crack Finder .....	29
4.3 Crack Segmentation Experiment .....	30
4.4 Noise Removal Experiment .....	34
4.5 Measuring Accuracy .....	38
4.5.1 Measuring Accuracy with Controlled Input Images .....	39
4.5.2 Measuring Accuracy with Mixed-characteristic Images from Real Survey .....	41
4.5.3 False Positive .....	45
4.5.3.1 Oil Stains .....	45
4.5.3.2 Objects on Road Pavement .....	46
4.5.3.3 Strong Texture and Illumination Problems .....	46
4.5.3.4 Wet and Noisy Images .....	47
4.5.3.5 Other Types of Distress .....	48
4.5.4 False Negative .....	49
4.5.4.1 Causes of False Negative in the Controlled Input Images .....	50
4.5.4.2 Cause of False Negative in the Mixed-Characteristic Input Images .....	50
4.5.4.3 Investigating of False Negative on the Mixed-Characteristic Input Images .....	56
CHAPTER V CONCLUSIONS AND RECOMMENDATIONS .....	58
5.1 Conclusions .....	58
5.2 Contributions .....	60
5.3 Limitations .....	60
5.4 Comments and Recommendations .....	61



	Page
References.....	62
Appendix .....	64
Appendix A Experimental Results.....	65
Appendix B Publication.....	69
Biography .....	76



# ศูนย์วิทยทรัพยากร จุฬาลงกรณ์มหาวิทยาลัย

## List of Tables

	Page
Table 4.1 Object Information for Figure 4.8.....	35
Table 4.2 Object Information for Figure 4.9.....	36
Table 4.3 Results of Measuring the Proposed Approach Accuracy with Controlled Input Images .....	40
Table 4.4 The Total Numbers of Each Distress Type.....	42
Table 4.5 The Total Number of Distressed Image Frames .....	43
Table 4.6 Results of Measuring the Proposed Approach Accuracy with Mixed- Characteristic Input Images .....	45
Table 4.7 Total Number of Distressed Images with False Positive Error.....	49
Table 4.8 Mixed-characteristic Input Images after Ignoring out of Scope Input Images .....	56
Table 4.9 Causes of False Negative in Mixed-Characteristic Input Images.....	56
Table 4.10 Causes of Crack Detection Fault.....	57
Table A.1 False Positive in Mixed-Characteristic Input Images .....	66
Table A.2 False Negative in Mixed-Characteristic Input Images .....	67
Table A.3 Investigation of False Negative in Mixed-Characteristic Input Images Excluding out-of-scope Images .....	68
Table A.4 Investigation of False Negative in Mixed-Characteristic Input Images Excluding out-of-scope Images and Human Fault .....	68

ศูนย์วิจัยทรัพยากร  
 จุฬาลงกรณ์มหาวิทยาลัย

## List of Figures

	Page
Figure 1.1	Example Images with Illumination and Texture Problems ..... 2
Figure 2.1	Examples of Dilation Operation [10] ..... 7
Figure 2.2	Examples of Erosion Operation [10] ..... 8
Figure 2.3	Examples of Opening and Closing Operation [10]..... 9
Figure 2.4	Grid Cell Attribute in Pavement Image..... 10
Figure 2.5	Hill Climbing Pseudo-code..... 11
Figure 3.1	Proposed Approach Flow Chart..... 13
Figure 3.2	Difference Grid Cell Size with its Border Brightness Profile ..... 14
Figure 3.3	Original Image ..... 15
Figure 3.4	Pre-processing Phase ..... 15
Figure 3.5	Crack Segmentation Flow Chart..... 16
Figure 3.6	Grid Cell Attribute above Edge of Shadow Area ..... 17
Figure 3.7	Grid Cell Attributes with Overlapping Area..... 18
Figure 3.8	Grid Cell Attribute with Strong Texture..... 18
Figure 3.9	Grid Cell Attributes with Crack Arrangement..... 19
Figure 3.10	Examples of Noise in Resulting Images of Segmentation Phase ..... 20
Figure 3.11	Enlarged Elements ..... 21
Figure 3.12	Crack Gravitation..... 22
Figure 3.13	Noise Removal Pseudo Code ..... 23
Figure 3.14	Examples of Crack Distress ..... 24
Figure 3.15	Result from Noise Removal Phase ..... 24
Figure 3.16	Merging Method ..... 25
Figure 4.1	Survey Vehicle [14]..... 27
Figure 4.2	Pavement View Cameras [14]..... 27
Figure 4.3	Exposure Problem ..... 28
Figure 4.4	Manual Distress Rating Part of CU Crack Finder Program..... 29
Figure 4.5	Automatic Distress Rating Part of CU Crack Finder Program ..... 30
Figure 4.6	Examples of Result Images..... 32

	Page
Figure 4.7 Experimental Result Images Compared with Original Algorithm with Same Variable Values .....	33
Figure 4.8 Considered Object (0) on a Crack Line .....	35
Figure 4.9 Considered Noise Object (0) .....	36
Figure 4.10 Noise Removal Result Images .....	37
Figure 4.11 Examples of Input Images for Measuring Accuracy.....	40
Figure 4.12 Examples of Input Pavement Images .....	41
Figure 4.13 Examples of Two Type of Distress in an Image.....	42
Figure 4.14 Vann Diagram of Distress Image Frames .....	43
Figure 4.15 Manual and Automatic Distress Rating.....	44
Figure 4.16 False Positive on the Images with Oil Lines .....	45
Figure 4.17 False Positive on the images with objects .....	46
Figure 4.18 False Positive on the Images with Strong Texture and Illumination Problems .....	47
Figure 4.19 False Positive on the Wet Pavement Images .....	47
Figure 4.20 False Positive on Noisy Image .....	47
Figure 4.21 False Positive on Crack and Other Types of Distresses.....	48
Figure 4.22 False Positive on Distressed Images. ....	49
Figure 4.23 Total Number of Distressed Image with False Positive Error.....	49
Figure 4.24 False Negative on Controlled Input Images.....	50
Figure 4.25 Linear Crack Rating.....	51
Figure 4.26 Interconnected Crack Rating .....	52
Figure 4.27 Rating with Wrong Type of Distress .....	53
Figure 4.28 Examples of Larger Crack Size.....	53
Figure 4.29 Examples of Smaller Size of Cracks .....	54
Figure 4.30 Noisy Input Images.....	55
Figure 4.31 Low Contrast Images.....	55
Figure 4.32 Examples of Classification Fault.....	57
Figure A.1 False Positive in Mixed-Characteristic Input Images.....	66
Figure A.2 False Negative in Mixed-Characteristic Input Images.....	67



## CHAPTER I

### INTRODUCTION

Highway management system is typically used for estimating the budget and for making maintenance plans. Like all systems, the input of correct data is essential. Submitting incorrect raw data can create circumstances that would cause grave financial distress to local, regional, and national governments.

When looking at the area of pavement distress, visual inspection by human inspectors is time consuming, requires too many professional inspectors, and is financially restrictive. Moreover distress classifications and measurement are subjective. Two inspectors may give different results of distress information even if they are looking at the same thing.

To solve these problems, an automatic crack monitoring system [1] is applied. This automatic system can be separated into two phases. In the first phase, the system collects road surface images using a camera installed on a survey vehicle. In the second phase, an automatic processing of collected images is performed to locate and measure distress.

A major problem of this automatic system is the accuracy of distress information from automatic processing. This problem is caused by the quality of collected images. Most systems up until now use area scan cameras which were installed on survey vehicles. The area scan camera captures an image of a certain size and resolution. The bigger the area covered, the more tendentious to have non-uniform illumination on an image.

To improve the quality of images, a research [2] recommended the use of line scan cameras with artificial light to give uniform illumination and to remove shadow in the images. Because one strip or width of the pixel was captured with enough light, the captured images were of good quality with uniform light and the crack lines were obvious to be noticed.

Even though, line scan seems to give better quality of road surface images, many old systems still use area scan cameras. Also, the need for better crack detection

algorithm for area scan images can come from the need to re-extract crack information of archived images. For example, studying about how cracks grow as time passed by needs accurate crack information from archived images. Therefore, suitable crack detection algorithm for area scan images is still necessary.

### 1.1 Crack Detection Difficulties

There are two major difficulties in crack detection process. The first difficulty is due to the surveying with an area scan camera in an open environment where light condition is a considerable problem. There is a lot of unavoidable shadow and shading

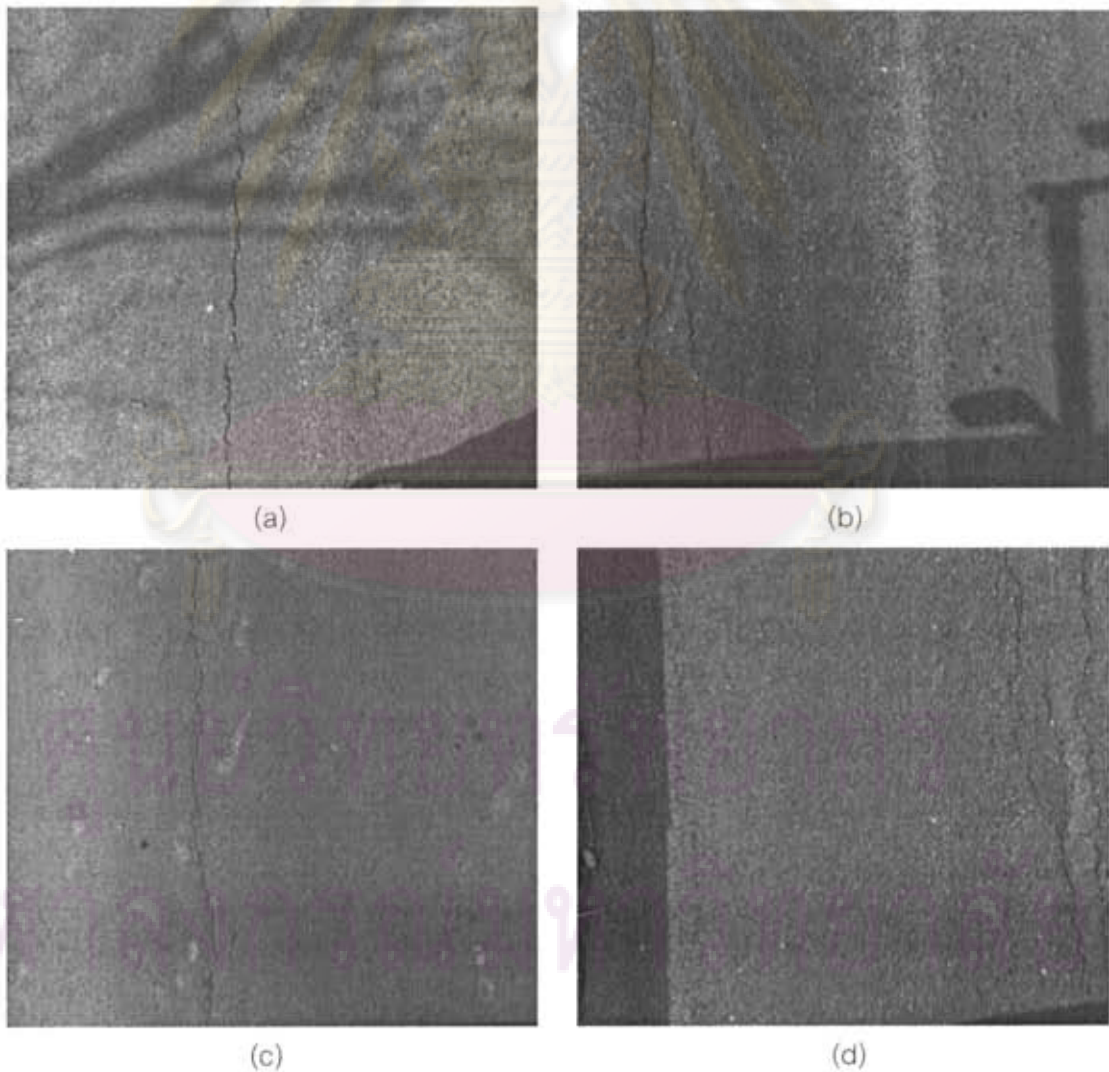


Figure 1.1 Example Images with Illumination and Texture Problems

in the images. Figure 1.1(a) shows unavoidable shadow from surrounding, e.g. tree branches. Figure 1.1(b) shows shadow from the survey vehicle. Moreover, an area scan camera cannot give uniform illumination images, even if there is no shadow. The image with illumination problem is shown in Figure 1.1(c)

The second important difficulty is due to the pavement texture. From the hypothesis, a crack is a narrow strip of pixels whose intensity is perceptible darker than the surrounding background. However, strong texture makes crack and background blend together, which is shown in Figure 1.1(d). It is easy for human to define crack area on strong texture images, but complicated for image processing.

## 1.2 Objective

The objective of this research is to develop an image processing algorithm based on Grid Cell Analysis technique for crack detection on asphaltic concrete road surface images.

## 1.3 Scope of Work

In this research, the focus is on image processing algorithm for crack detection on asphaltic concrete road surface images. The scope of work is defined as follow.

1. The result of the proposed algorithm is crack information which consists of types of cracks and their bounded areas.
2. Two types of cracks, linear cracks and interconnected cracks are considered in this research.
3. Cracks which are approximately three-pixel in strip width are considered.
4. In crack identification phase, a user has to define crack characteristics for each type of cracks.
5. The accuracy of the proposed algorithm will be checked by expert inspectors.
6. The proposed algorithm cannot handle images of roads which are covered with objects.

7. The proposed algorithm is not for use with underexposed or overexposed images.
8. The proposed algorithm is for use with dry asphaltic concrete road surface images.

#### 1.4 Workflow

1. Study asphaltic concrete surface characteristics, includes crack characteristics and other type of distress characteristics.
2. Study Grid Cell Analysis (GCA) [3] and other related works.
3. Implement GCA [3] method to example surface images with crack and non-crack area.
4. Design enhanced grid cell analysis algorithm.
5. Design noise removal algorithm.
6. Implement the proposed algorithm to example surface images.
7. Analysis the result.
8. Conclusion and composing the thesis.

ศูนย์วิทยทรัพยากร  
จุฬาลงกรณ์มหาวิทยาลัย



## CHAPTER II

### LITERATURE SURVEY AND THEORY STATEMENTS

#### 2.1 Literature Survey

From the difficulties in crack detection process, many researches were done to solve these problems. For example, an inspection system with image processing algorithm for detecting cracks in a tunnel [4] was proposed. This algorithm applied Sobel and Laplacian operators to find crack edges. It applied a graph search method to find crack line from two points in an image. However, this system was semi-automatic, which needs the starting point and the ending point of each crack indicated by user. In addition, this system was applied to the indoor structure, e.g. a road tunnel wall, or a subway tunnel wall. The characteristics of these walls were different from the characteristics of asphalt surface.

Another example of crack detection technique is morphological operation. There is a research applying this technique to high-grade highway pavement images [5]. The algorithm with enhancement step used median filter algorithm with multi – structure elements. Then crack edges were extracted by closing operation and the crack edges were thinned by erosion operation in order to get the length and width of cracks. Compared with other methods that use edge detection algorithm, the algorithm used less processing time. However, it was only applied to high – grade highway pavement images.

Artificial Intelligence is another method for finding crack areas. In 2004, there was a proposed method [6] using artificial living system to remove noise, oil stains, and dark spots. A study, by Tomikawa, was based on the basics of appropriate template matching controlled by a genetic algorithm [7]. And there was a research report [8] using a neural network to identify cracks by analyzing images extracted from video sequences. Artificial Intelligence techniques give good results. However, those techniques need a large training data set which takes a lot of time to construct and the training time is very long.

In 2006, a wavelet-based image processing method was also applied in automation for crack detection on pavement surface image [9]. The idea of using wavelet-based was to define the most adapted mother wavelet function for various pavement textures. In the same year, Huang and Xu [3] presented an image processing algorithm for inspection of pavement cracking based on grid cell analysis (GCA). Their research consisted of three main steps. The first step was called grid cell analysis. In this step, the pixels that were chosen as crack cells were regarded as a crack seed. The second step verified a crack seed by using the contrast of a crack seed to its neighbors. The last step was crack cluster connection. This step connected individual seeds into seed clusters for crack identification in a later step. Nevertheless, this algorithm is suitable for images from line scan cameras with uniform artificial light. In addition, this solution needs preset thresholds that are not suitable for non-uniform illumination images.

## 2.2 Morphological Image Processing in Grayscale Image

The word morphology commonly denotes a branch of biology that deals with the form and structure of animals and plants. In the context of image processing [10, 11] it is the name of a specific methodology designed for the analysis of the geometrical structure in an image. The morphology techniques are useful in the representation and description of region shape. Moreover, these techniques are helpful in pre- or post-processing.

Morphological image processing is a set of techniques for digital image processing based on mathematical morphology. The language of mathematical morphology is set theory. Mathematical morphology examines the geometrical structure of an image by probing it with small patterns, called 'structuring elements', of various sizes and shapes. Since these techniques rely only on the relative ordering of pixel values, not on their numerical values, they are especially suited to the processing of binary images and grayscale images whose light transfer function is not known.

In grayscale images, digital image functions are shown in the form of  $f(x, y)$  and  $b(x, y)$ , where  $f(x, y)$  is an input image and  $b(x, y)$  is a structuring element.

## 2.2.1 Dilation and Erosion Operations

Dilation and erosion operations are fundamental to morphological processing. Many morphological algorithms are based on these two primitive operations. These basic operations produce contrasting results when applied to either grayscale or binary images. Dilation and erosion have a different effect on an image. Erosion shrinks image objects while dilation expands them. The specific actions of each operation are covered in the following sections.

### (1) Dilation Operation in Grayscale Image

Grayscale dilation of input image  $f$  by structuring element  $b$ , denote  $D(f,b)$ , is defined as

$$D(f,b)(s,t) = \max\{f(s-x,t-y) + b(x,y) \mid (s-x),(t-y) \in D_f; (x,y) \in D_b\}$$

Where  $D_f$  and  $D_b$  are the domain of  $f$  and  $b$ , respectively. Dilation generally increases the sizes of objects, filling in holes and broken areas, and connecting areas that are separated by spaces smaller than the size of the structuring element. With grayscale images, dilation increases the brightness of objects by taking the neighborhood maximum when passing the structuring element over the image. The dilation images with 3x3 rectangle shape structuring element are shown in Figure 2.1.

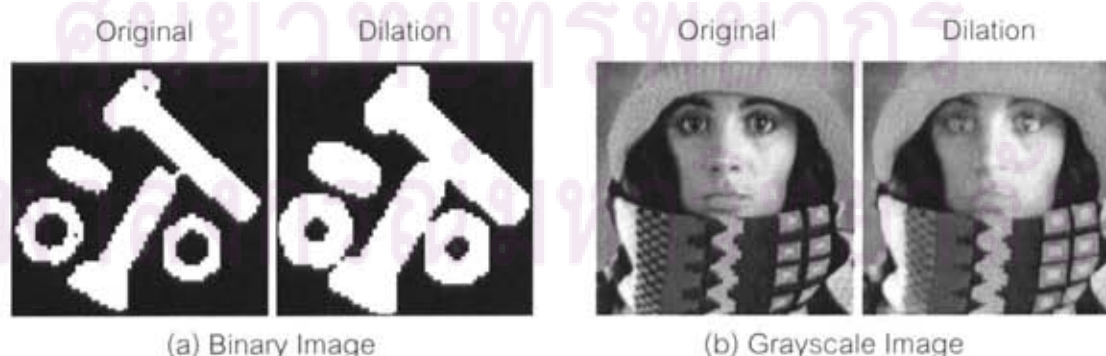


Figure 2.1 Examples of Dilation Operation [10]





Figure 2.2 Examples of Erosion Operation [10]

## (2) Erosion Operation in Grayscale Image

Grayscale erosion of input image  $f$  by structuring element  $b$ , denote  $E(f, b)$ , is defined as

$$E(f, b)(s, t) = \min\{f(s+x, t+y) - b(x, y) \mid (s+x), (t+y) \in D_f; (x, y) \in D_b\}$$

Where  $D_f$  and  $D_b$  are the domain of  $f$  and  $b$ , respectively. Erosion generally decreases the sizes of objects and removes small objects by subtracting objects with a radius smaller than the structuring element. With grayscale images, erosion reduces the brightness and size of bright objects on a dark background by taking the neighborhood minimum when passing the structuring element over the image. The examples of erosion with 3x3 rectangle shape structuring element were shown in Figure 2.2.

### 2.2.2 Opening and Closing Operations

Erosion and dilation can be used in a variety of ways, in parallel and series, to give other transformations. Two very important transformations are opening and closing.

Opening generally smoothes a contour in an image, breaks narrow isthmuses and eliminates thin protrusion. Closing tends to narrow smooth sections of contours, blend narrow breaks and long thin gulfs, eliminate small holes, and fill gaps in contours.

The Opening of input image  $f$  by structuring element  $b$ , denote  $O(f, b)$ , is defined as



$$O(f,b) = D(E(f,b),b)$$

It can say that the opening  $f$  by  $b$  is the erosion of  $f$  by  $b$ , followed by a dilation of the result by  $b$ .

Similarly, the closing of input image  $f$  by structuring element  $b$ , denote  $C(f,b)$ , is defined as

$$C(f,b) = E(D(f,b),b)$$

Thus, the closing  $f$  by  $b$  is the dilation of  $f$  by  $b$ , followed by an erosion of the result by  $b$ . The examples of opening and closing operations are shown in Figure 2.3.

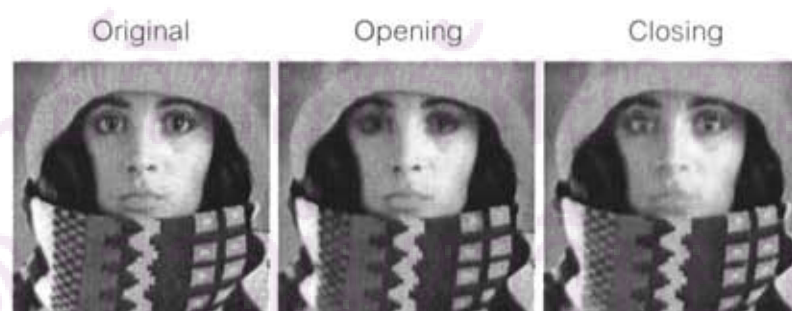
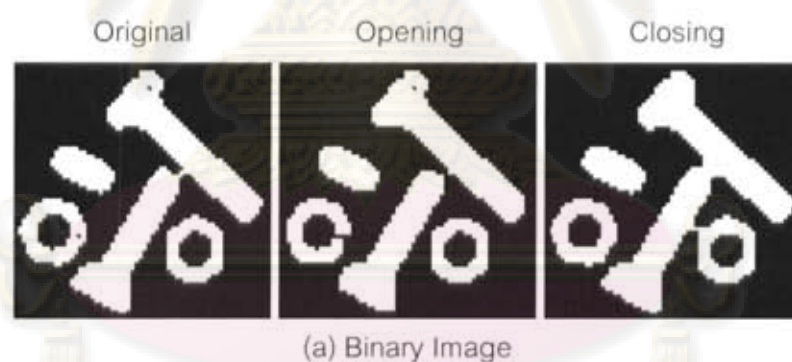


Figure 2.3 Examples of Opening and Closing Operation [10]

### 2.3 Grid Cell Analysis (GCA)

Grid Cell Analysis (GCA) [3] is a technique for crack segmentation. Instead of looking for crack line in whole image, GCA looks for a crack characteristic in a small part of image which is a "grid cell".

In this technique, a pavement image was divided into grid cells of 8x8 pixels and each grid cell was classified as crack or non-crack cell using the grayscale information of the border pixels as shown in Figure 2.4.

The first column in Figure 2.4 shows the original image, the second column shows the enlarged grid cells and the last column shows the border brightness profiles where two strips represent one side of the grid cell.

A crack cell is identified by comparing its features from crack information to preset thresholds. Crack information includes the length, the width, and the contrast of a dark object. It also includes mean brightness, minimum brightness, and the presence of a dark strip within the cell, which is the valley in the border brightness profile. When a cell does not contain a crack, its border profile shows no apparent valley as shown in Figure 2.4(a). In Figure 2.4(c), the border profile shows two sharp valleys, indicating the crossing points of a crack on the border. Figure 2.4(b) shows only one significant valley in the border grayscale, the cell may have edge crack. The result of grid cell analysis is a seed point which is the darkest spot in the cell.

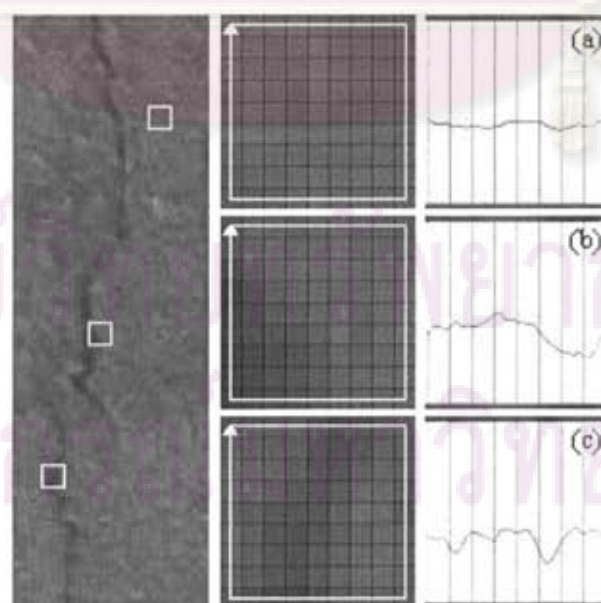


Figure 2.4 Grid Cell Attribute in Pavement Image

Nevertheless, this algorithm is suitable for images from line scan camera with uniform artificial light. In addition, this solution needs preset thresholds that are not suitable for non-uniform illumination images.

## 2.4 Hill Climbing Algorithm

The simplest way to implement heuristic search is through a procedure called hill climbing [12]. In hill climbing strategy, the basic idea is to always head towards a state which is better than the current one. This strategy might be used as an eager but blind mountain climber who goes uphill along the steepest possible path until he can go no farther up. Because it keeps no history, the algorithm cannot recover from failures of its strategy. Hill climbing can be described as a pseudo-code in Figure 2.5.

1. Start with *current-state* = *initial-state*.
2. Until *current-state* = *goal-state* OR there is no change in *current-state* do:
  - 2.1 Get the children of the *current-state* and use the evaluation function to assign a score to each child.
  - 2.2 If one of the children has a better score than the *current-state* then set the new *current-state* to be the child with the best score.

Figure 2.5 Hill Climbing Pseudo-code

A major problem of hill climbing strategy is their tendency to become stuck at local maxima. If they search state that has a better evolution than any of its children, the algorithm stops. If this state is not a goal, but just a local maximum, the algorithm may fail to find the best solution. Because "better" need not be "best" in an absolute sense. The algorithm is unable to distinguish between local and global maxima.

## 2.5 Law of Gravities

Gravitation [13] is a natural phenomenon where all objects with mass attract each other with a force of gravitational attraction. Gravitation is responsible for keeping the Earth and the other planets in their orbits. It is also the reason for the very existence of the Earth, the Sun, and all objects in the universe.

Modern physics describes gravitation using the general theory of relativity, but the much simpler Newton's law of universal gravitation provides an excellent approximation in most cases.

The Newton's theory of universal gravitation states that:

"Each particle of matter attracts every other particle with a force which is directly proportional to the product of their masses and inversely proportional to the square of the distance between them."

The standard formula for gravity is:

$$\text{Gravitational force} = G \frac{m_1 m_2}{d^2}$$

Where  $G$  is the gravitational constant,  $m_1$  and  $m_2$  are the masses of the two objects and  $d$  is the distance between the centers of gravity of the two masses.

From the standard formula, consider the gravitational force between object A and object B. The force exerted on object A by object B is equal and opposite of the force on object B by object A. If the mass of object A was doubled, the force on object B would double. Likewise, if the mass of object B was doubled, the force on object A would double. Finally, if object A was twice as far away from object B, the force on object A would be a factor four smaller.

จุฬาลงกรณ์มหาวิทยาลัย



### CHAPTER III RESEARCH METHODOLOGIES

In this chapter, the process of crack detection is described. The approach can be viewed as four phases. The first phase is the pre-processing phase which is for improving original images. The second phase is the crack segmentation which extracts crack objects from the original images. The next phase is the noise removal phase which is used for increasing the accuracy of the crack identification algorithm. The last phase is the crack identification phase which is used for classifying crack type. After this phase, the output distress data can then be used in highway management system. The flow chart of this approach is shown in Figure 3.1.

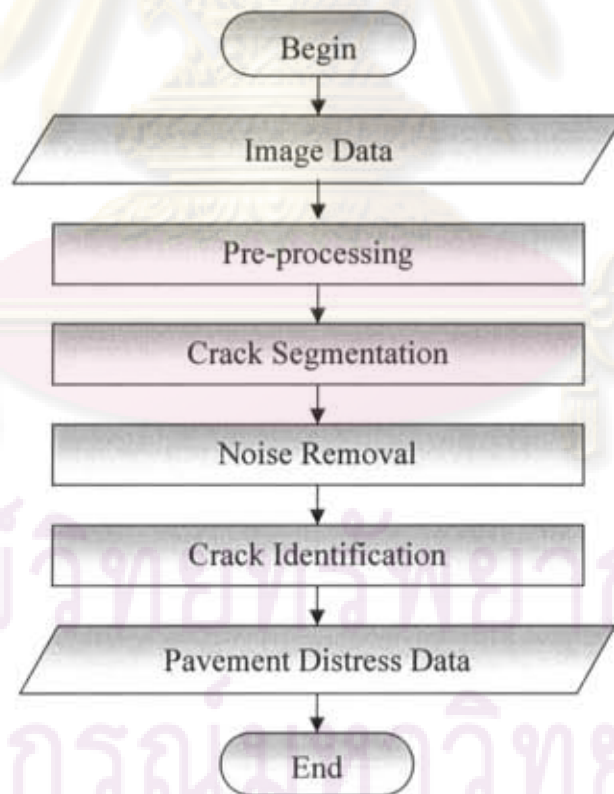


Figure 3.1 Proposed Approach Flow Chart

### 3.1 Grid Cell Size

This research was intended to use the highway pavement image dataset already on hand as the test dataset. The resolution of a pixel was 1.8 millimeters and most crack body of five millimeters showed up on most crack images. Choosing a grid cell size was important for grid cell analysis. Bigger or smaller grid cell size may not show enough information of the crack. Figure 3.2 shows grid cells of the same crack area in an image. The grid cells are shown in three different sizes with corresponding border brightness profiles. With small grid cell, as shown in Figure 3.2(a), there is no noticeable valley in the profile. Figure 3.2(c) shows the cell whose size is too big. It gives many valleys, thus the crossing points of a crack on the border are indistinct. The proper profile should have two clear-shape valleys as shown in Figure 3.2(b).

The grid cell size is also related to the crack width or the width of the dark strip. The proper grid cell size should give distinct crack in an image. For the dataset on hand, the grid cell size should be approximately three times the crack width which is nine pixels in width and height. In this research, a grid cell size of 9x9 was used.

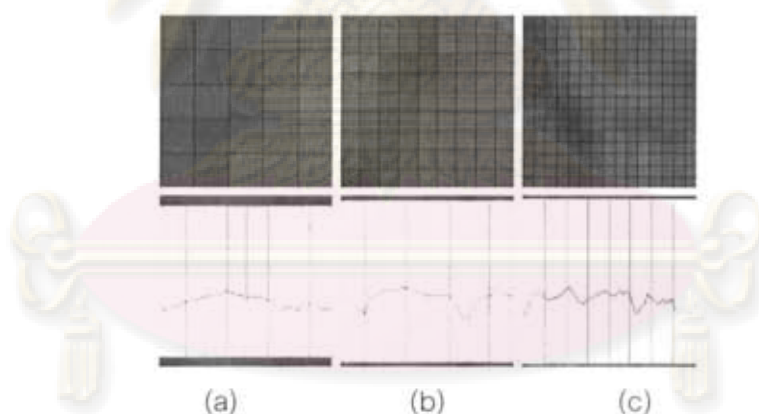


Figure 3.2 Difference Grid Cell Size with its Border Brightness Profile

### 3.2 Pre-processing Phase

Generally, the asphaltic concrete road surface images from a survey camera may contain faded and disconnected cracks including many black and white spots. Figure 3.3 is an example of this situation which perplexes the algorithm when encountering the dark strip objects. In order to enhance the cracks, i.e. to make them unbroken and to remove noise, morphological operations in gray-scale images are

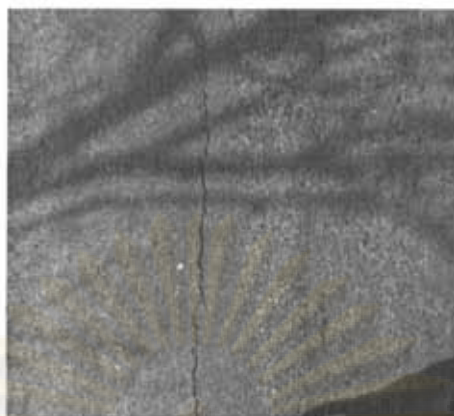


Figure 3.3 – Original Image

applied to improve the original image. This technique connects the dark pixels together, and removes isolated dark spots.

To improve the original images according to the above methods, two steps of morphological techniques are applied. First, opening technique is applied to the original image. This technique helps connect pieces of crack line together. Moreover, this technique makes a crack line become darker and be simpler to be noticed by the algorithm.

The second step of the pre-processing phase is closing technique. Although the opening technique gives an obvious crack line, black noise spots are also darker. Closing technique is used to remove the small dark spots which are smaller than structure element.

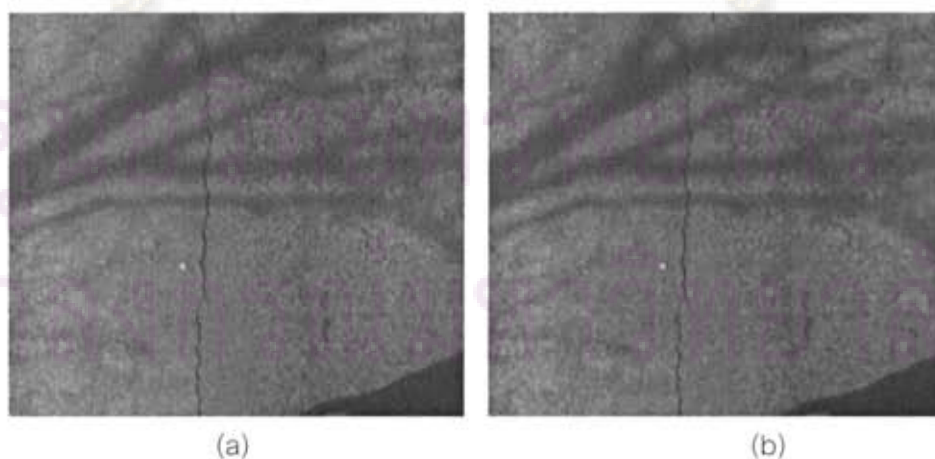


Figure 3.4 Pre-processing Phase

For example, when apply the opening technique is applied to the original image in Figure 3.3, the darker crack line, which is shown in Figure 3.4(a), becomes clearly visible. However, black noise spots also get darker. Figure 3.4(b) shows the final state of pre-processing phase which performs the closing technique on the Figure 3.4(a). The spots which are darkened from the first phase are disappeared. As a result, only crack line can be perceived easily with less noise.

The structure element in morphing is in a square shape with the size of one-third of the grid cell width. Since grid cell size is related to crack size, the structure element of this size can remove dark spots which are smaller than the structure element and can also emphasize the crack.

### 3.3 Crack Segmentation Phase

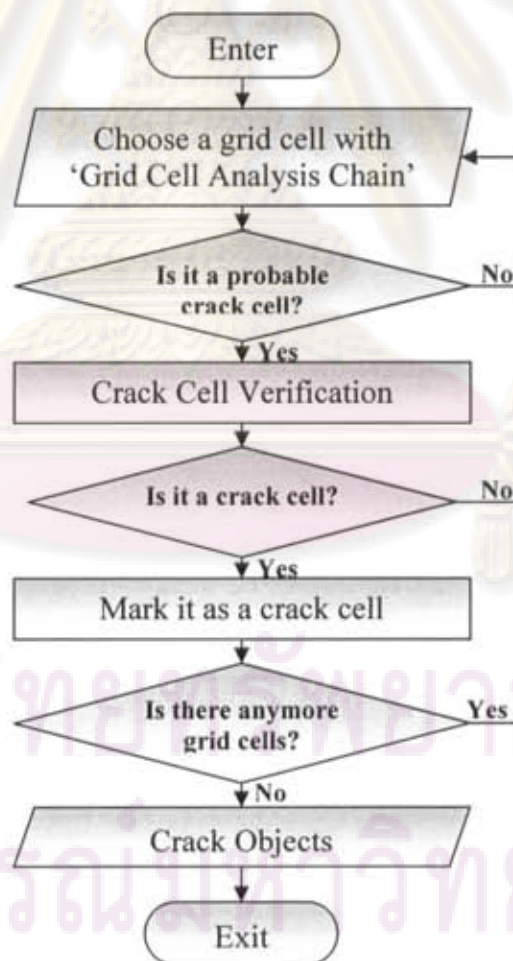


Figure 3.5 Crack Segmentation Flow Chart



The crack segmentation phase is based on using GCA to classify a crack cell, but the proposed algorithm has been enhanced for assuring the possible crack cell. Additionally, this approach uses heuristic decision on classifying crack cell instead of using preset thresholds for the purpose of dealing with illumination problem.

This phase can be separated into two parts. The first part is the grid cell analysis chain which handles shadow problems. And the other part is the crack cell verification which guarantees the crack cells. The crack segmentation flow chart is shown in Figure 3.5.

### 3.3.1 Grid Cell Analysis Chain

From the GCA, a pavement image is divided into grid cells which are classified as crack or non-crack cells. In contrast to GCA method which needs preset thresholds, this approach uses the border brightness profile with hill climbing technique to find the valleys in order to cope with the non-uniform illumination problem.



Figure 3.6 Grid Cell Attribute above Edge of Shadow Area

In many cases, when images contain a shadow, a profile with one significant valley may not always be a crack cell. As shown in Figure 3.6, a grid cell covering the edge of shadow area gives the profile that looks like the edge crack in Figure 2.4(b). To avoid this problem, instead of using two cases of profiles to indicate a crack cell, the profile, which might be the crack cell, must show only two considerable valleys, otherwise it is likely to be a non-crack cell.

However, the above method would eliminate the cells that have edge crack. As a result, double checking on images is necessarily applied. After divided into grid cells, the original image is divided again in overlapping area as given in Figure 3.7. This method can extract the crack area and keep away from the edge of shadow.

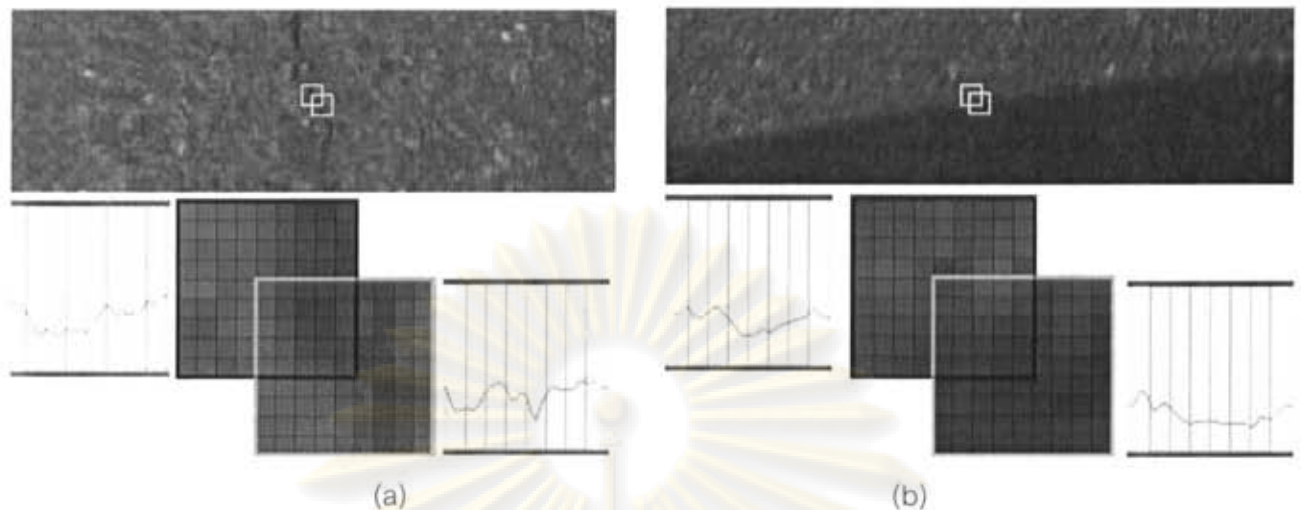


Figure 3.7 Grid Cell Attributes with Overlapping Area

Figure 3.7 shows an overlapping area over different surfaces. Figure 3.7(a) is an image over a crack area while Figure 3.7(b) is an image over a shadow area. Both profiles in the left side of Figure 3.7 look quite similar with one significant valley, which means they are non-crack cells. Consequently, crack area in Figure 3.7(a) is ignored. After shifting the cell, the right profile in Figure 3.7 (a) shows two significant valleys while the right profile in Figure 3.7(b) shows only one. That is, the crack area in Figure 3.7(a) is extracted, whereas the shadow area is not.

### 3.3.2 Crack Cell Verification

Strong texture is another problem that reduces the accuracy of crack detection algorithm. Figure 3.8 shows a non-crack cell which has a profile similar to a crack profile.

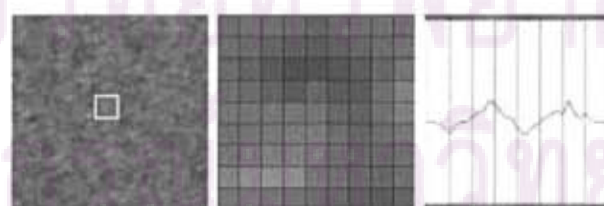


Figure 3.8 Grid Cell Attribute with Strong Texture

From the basic concept, a border profile which shows two sharp valleys indicates that there are two crossing points of a crack on the border, but it does not guarantee that a crack is in the cell as shown in Figure 3.9(a). To ensure that a crack is in the cell, it must be further examined. If there are dark pixels arranging in a line between two valleys, the cell is verified as a crack cell.

To verify the crack cell, all distances between each dark pixel to the imaginary line between two crossing points of a crack on the border of a grid cell must be within the crack size. Figure 3.9 shows arrangements of dark pixels and the imaginary line. The dark pixels in Figure 3.9(a) are not adjacent to the imaginary line whereas the dark pixel arrangement in Figure 3.9(b) closely resembles the line.

The distance  $d$  between dark point  $p(x, y)$  and the imaginary line, point  $q(x_1, y_1)$  and point  $q(x_2, y_2)$ , is shown below.

$$d = \sqrt{(x - x_c)^2 + (y - y_c)^2}$$

Where 
$$x_c = \frac{m^2 x_1 - m y_1 + m y_2 + x_2}{m + 1}$$

$$y_c = m x_c - m x_1 + y_1$$

$$m = \frac{y_2 - y_1}{x_2 - x_1}$$

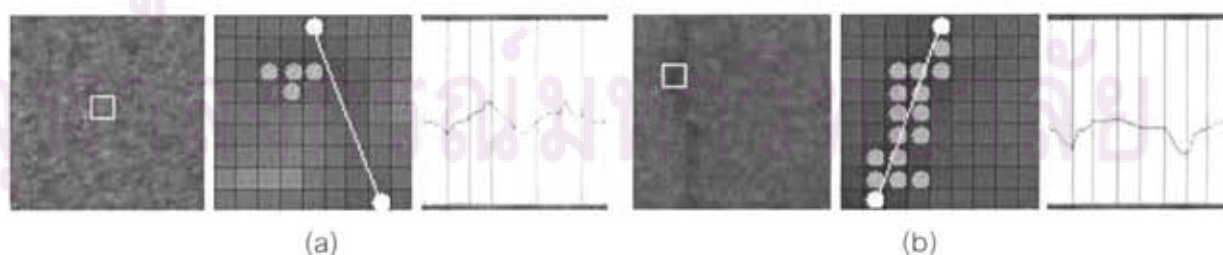


Figure 3.9 Grid Cell Attributes with Crack Arrangement

### 3.4 Noise Removal Phase

Even though the proposed method in segmentation phase can solve non-uniform illumination and strong texture problem, there is still some noise in the result from segmentation phase. This noise is a problem for classifying crack type. Unlike white noise or salt and pepper noise, this type of noise cannot use filter to remove it. The noise is a small object and looks like small piece of crack, thus crack and non-crack objects are blended together. As a result, it is difficult to identify the crack area.

Figure 3.10 shows the resulting images from the segmentation phase with noise objects. The noise came from dark spots on the original image as shown in Figure 3.10(a). Other types of pavement distress may also give noise. For example, Figure 3.10(b) shows an original image with patching which gives the resulting image too much noise.

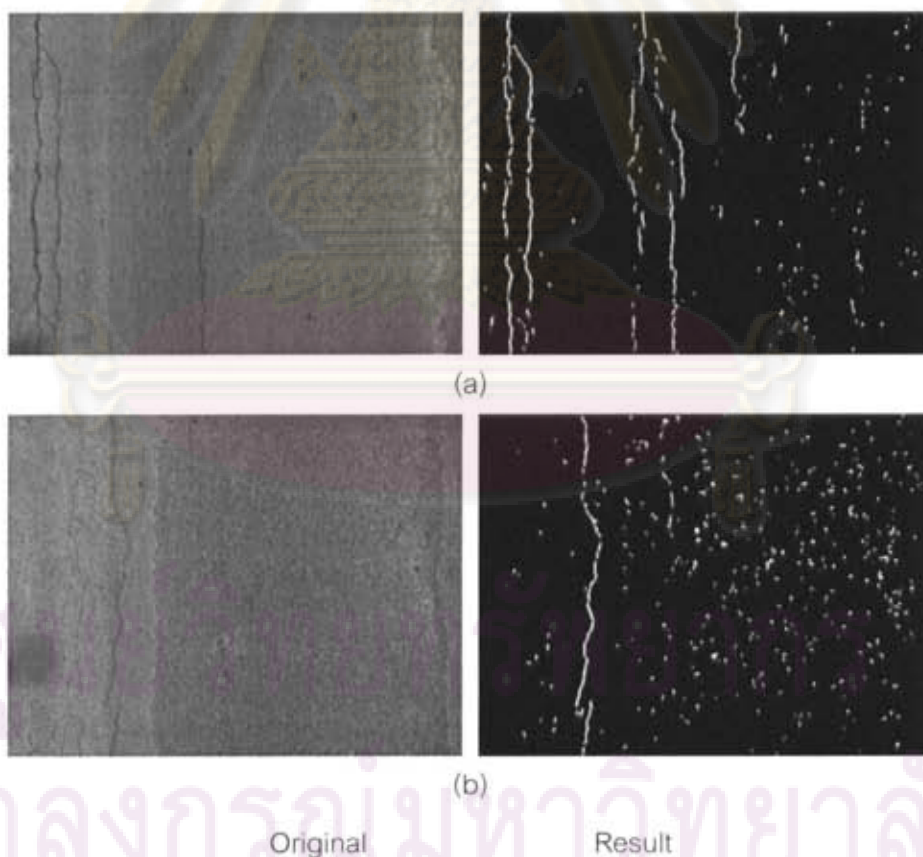


Figure 3.10 Examples of Noise in Resulting Images of Segmentation Phase



### 3.4.1 Crack Appearance

From segmentation processed images, an object is mostly justified to be a crack if it has a large area (pixel counts), but this is not always true. For example, large objects (a), (e), and (g) in Figure 3.11(a) are parts of crack lines, but many small objects in Figure 3.11(a) are also parts of crack lines too.

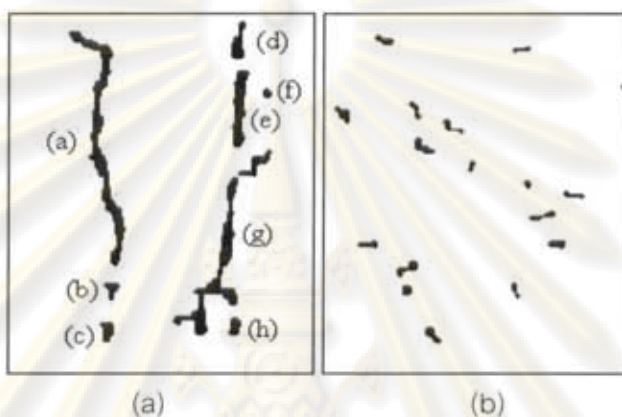


Figure 3.11 Enlarged Elements

In contrast to Figure 3.11(a), Figure 3.11(b) shows noise objects on non-crack area. However, these objects look like small objects in Figure 3.11(a), e.g. object (b), (c), and (h). The distinction between the small objects in Figure 3.11(a) and Figure 3.11(b) is the dispersal of the objects themselves. Small objects in Figure 3.11(a) are close to huge objects, while the objects in Figure 3.11(b) spread over the whole region. From this distinction, the technique for telling the difference between crack and non-crack objects was proposed with a supposition that a crack object is an object which has large area or stays close to a large object.

### 3.4.2 Gravitation Feature

Like force of gravitational attraction which attracts all objects together, a crack object is considered as part of a crack line or not by its area and the distance between it and other neighboring objects. For the purpose of noise removal, gravitation feature is

applied to calculate gravitational force between each pair of objects. If the force is strong enough, it indicates that the object is close to a large object and is considered a crack.

If object A has pixel area  $a_a$  and object B has pixel area  $a_b$ , then the magnitude of gravitational force feature  $f$  on object A is directed toward object B is shown below,

$$f = \frac{a_a a_b}{r^2}$$

where  $r$  is the shortest distance between the tips of object A and B.

Since the gravitational force is directly proportional to the pixel area of both interacting objects, more large objects will attract each other with a greater gravitational force. In contrast to the area, the force is inversely proportional to the shortest distance between the tips of the two objects. Farther distance will result in weaker gravitational forces.



Figure 3.12 Crack Gravitation

Due to the fact that most crack objects are narrow and almost aligned, the center of gravitation is then applied to the tips of the objects, as shown in Figure 3.12, in order to increase gravitational force to the surrounding objects. With this concept, the

gravitational force abruptly changes with the distance, thus, make it easier to perceive an object as a crack.

In order to classify crack, the area and the gravitational force are considered. Large area objects or strong gravitational forces are signs of crack objects. Otherwise, the objects are indicated as noise. In other words, weak gravitational forces show a characteristic of disorder arrangement of small objects.

```

Read Crack Objects from Crack Segmentation Phase
For each object A in Crack Objects
    For each object B in Crack Objects
        Calculate Gravitation Feature between Object A and Object B
        Store Gravitation Feature in Gravitation Feature Array.
    End For
    If there is at least one peak in the Gravitation Feature Array
        Set Object A as Crack Object
    Else
        Set Object A as Noise
End For
  
```

Figure 3.13 Noise Removal Pseudo Code

The pseudo code of distinguishing crack objects from noise objects is shown in Figure 3.13. The input of this phase is crack objects from crack segmentation phase. Gravitation features of each pair of crack objects are calculated. For each object, if there is at least only one peak in the set of gravitation features, the object is considered as a crack object. Otherwise, it is considered as a noise.

### 3.5 Crack Identification Phase

Crack objects from crack segmentation and noise removal phase are spread over the area. To classify the crack, geometric characteristics are used. In this research,

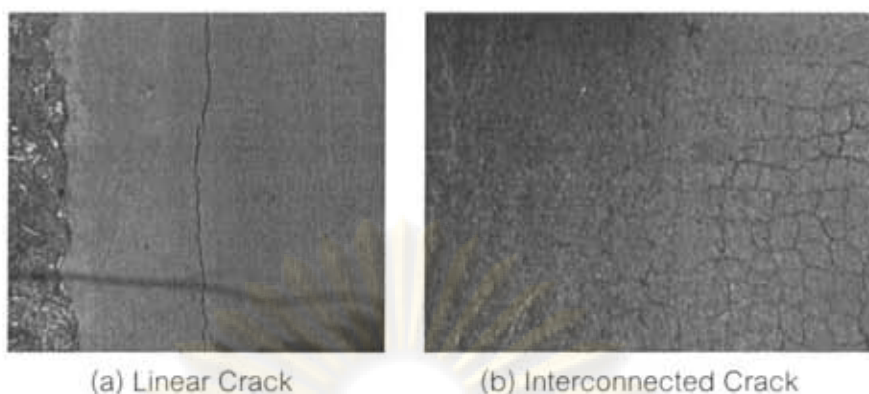


Figure 3.14 Examples of Crack Distress

two types of crack are considered. The first one is linear crack as shown in Figure 3.14(a) and the other one is interconnected crack as shown in Figure 3.14(a).

### 3.5.1 Merging Method

The results from noise removal phase are crack objects shown in Figure 3.15. A crack line can be performed by a group of cracks which lay next to one another. When looking at each object, it cannot give crack distress information which is crack type, its bounding area and its position. As a result, merging those objects into one is importance for crack identification.

To merge the objects together, convex hulls technique is applied to each object to find the smallest convex polygon containing all the points of the object. The points

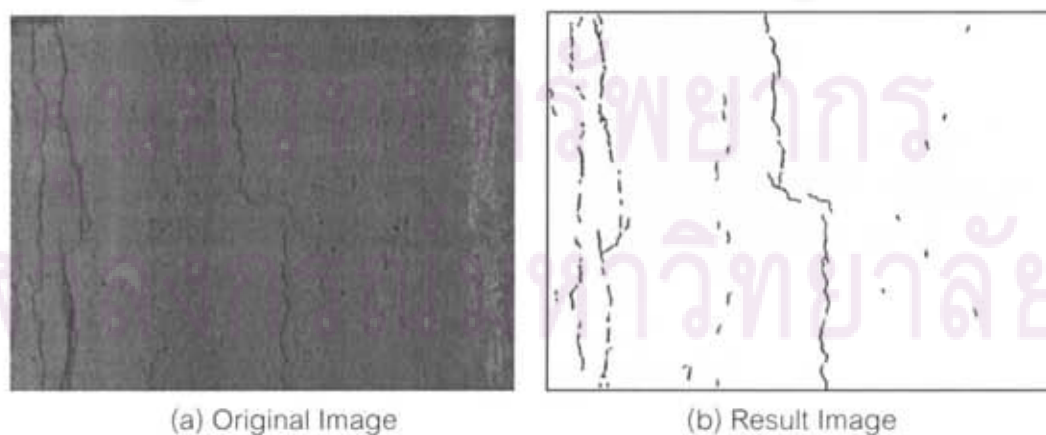


Figure 3.15 Result from Noise Removal Phase



from convex hull technique represent the object in term of geometric shape. The next step is computing the rectangle with minimum circumference rectangle, as shown in Figure 3.16(a), which contains all the points of each object. This rectangle gives object information, i.e. its length, its width, and its rotational angle.

Due to the fact that most crack objects are close and almost arrange in a line, the objects which probably assemble a crack line have some area that lay on other objects. For this reason, the rectangles of each object are expanding their height in order to raise the possibility of overlapping area.

After expanding the heights, each rectangle is filled, as shown in Figure 3.16(b), and convex hulls technique is then applied to fine the rectangle with minimum circumference rectangle again. Figure 3.16(c) shows the result of merging method. The result object gives enough crack distress information to identify crack.

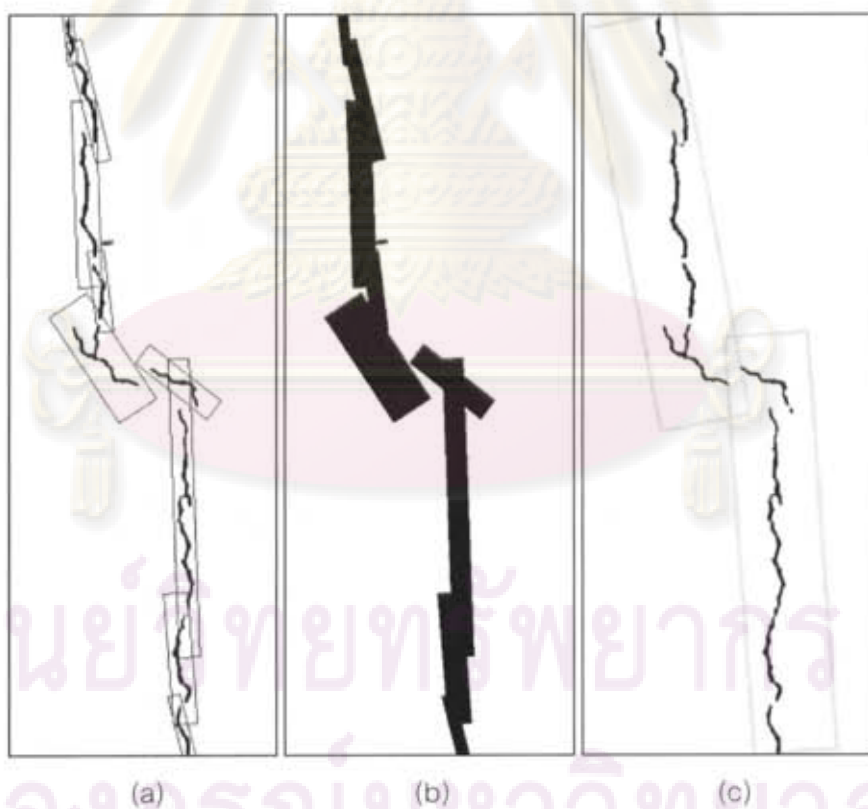


Figure 3.16 Merging Method

### 3.5.2 Geometric Characteristics

The results from merging method are objects with geometric characteristics which are the center point, the height, the width, and the rotational angle. It also includes the area and the circumference of the object. These characteristics are used to identify crack type. For example, if an object is narrow, that is two parallel sides of the rectangle are extremely longer than the others, the object is justified as a linear crack. Otherwise, it is an interconnected crack.

However, crack identification is ambiguous to justify even if professional inspectors do it themselves. For the most precise result, the user has to define the crack characteristics, e.g. crack size, and crack area.



ศูนย์วิจัยทรัพยากร  
จุฬาลงกรณ์มหาวิทยาลัย

## CHAPTER IV

### EXPERIMENTS AND EXPERIMENTAL RESULTS

#### 4.1 Data Resource / Data Collection

The images used in this research were from road survey database [14]. The survey of road pavement distress was done in the north part of Thailand by Department of Highway, Ministry of Transport, and CERT, Chulalongkorn University. The system used in the survey was installed in a van, as shown in Figure 4.1. The survey vehicle contained computers and survey equipment, such as laser profilometer, a GPS receiver, a gyroscope, asset view cameras and pavement view cameras.



Figure 4.1 Survey Vehicle [14]

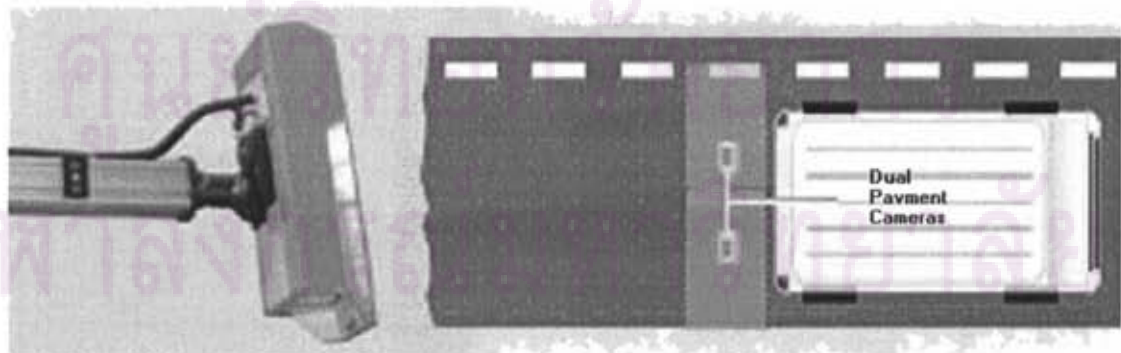


Figure 4.2 Pavement View Cameras [14]

With the intention to find crack distress, pavement images were used as the input for this research. The images were captured from area scan cameras installed at the back of the vehicle with an approximate coverage area of 2.40 x 1.75 square meters for each camera. The pavement images were captured with a resolution of 1024 x 960 pixels 8 bits gray-level and compressed with MJPG format. With these configurations, an image had a ground resolution of about 1.8 mm/pixel.

Though a camera covered 1.86 meters in width, a highway lane width is about 3.5 – 4 meters. In order to capture a full width of a lane, two area scan cameras were installed at the back of the survey vehicle, as shown in Figure 4.2. Both cameras captured pavement images using the same GPS position while the vehicle was moving. Then image processing was applied to correct camera distortion and to stitch the two images together. A stitched pavement image covered 4 x 1.75 square meters which sometime covered pavement shoulder.

Using two cameras instead of one to capture images gave better images in terms of ground resolution, however, it has some problems. For instance, images from both cameras might have different light intensity, as shown in Figure 4.3, and thus stitching the two images together might not give a good blend of the two images. Stitching images by blending technique seems to give a good-looking result to human vision but some crack information may be lost. In this research, the input images from both cameras were processed separately to keep the highest level of crack lines' detail and to avoid the problem of difficult exposure.

However, there were some areas in the image, as shown in Figure 4.2, that were not completely separated. In order to eliminate the overlapped area, instead of blending, the input images from both cameras needed to be cropped.

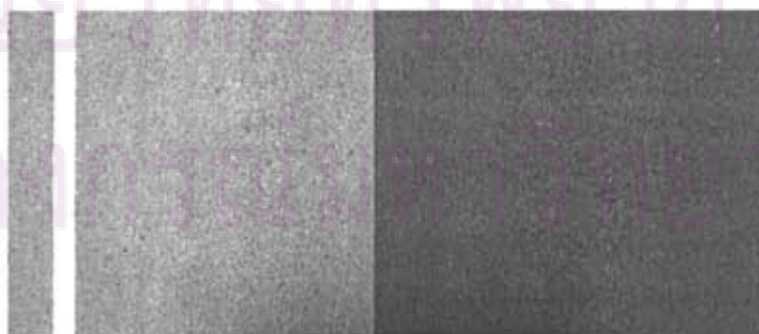


Figure 4.3 Exposure Problem



## 4.2 CU Crack Finder

CU Crack Finder is software developed by faculties and students at Chulalongkorn University. It was designed to handle the data sets of unique data structure, from the survey vehicle. The data sets consisted of several data, for example, pavement frame information, asset view frame information, GPS information and instrument sections. All data were linked by timestamp. CU Crack Finder estimated the relations between all data.

CU Crack Finder process could be separated into two parts, manual distressed rating and automatic distressed rating. Both parts were developed for the same purposes, i.e. estimating crack bounded areas and locating crack positions. However, the methods were different but in different methods.

In manual distress rating, pavement images were carefully monitored by professional inspectors. Because this part was designed according to inspectors' requirements, the user interface of this part was easy to use, so crack bounded area was approximately estimated. The user interface consisted of asset view images from three cameras (installed on the front roof top of the survey vehicle), GPS information and pavement view images (which were assembled as a continued road image). The interface is shown in Figure 4.4.



Figure 4.4 Manual Distress Rating Part of CU Crack Finder Program

Unlike manual distress rating part, the user interface in automatic rating part consisted of start and stop buttons. The input images were sent to the algorithm automatically, and the output was stored in the data base. The user interface is shown in Figure 4.5.

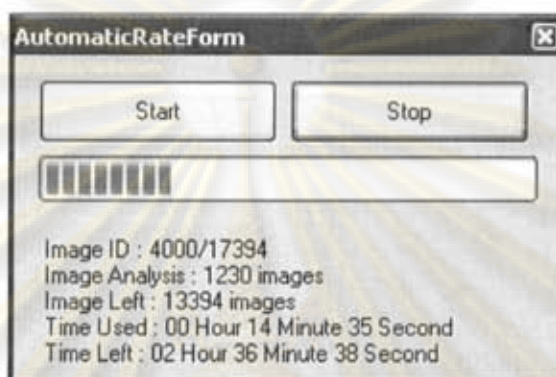


Figure 4.5 Automatic Distress Rating Part of CU Crack Finder Program

### 4.3 Crack Segmentation Experiment

Crack segmentation phase was improved from Huang and Xu's approach [3]. The original approach had been applied to the pavement images from line scan cameras with artificial light to improve their quality. The images from line scan cameras were brighter, had lower distortion, and had more contrast between cracks and background. In contrast to the original method, this research had been developed to cope with pavement images from area scan cameras which might contain non-uniform illumination and shadow problems

In order to evaluate the effectiveness, the proposed crack segmentation phase was compared to the Huang and Xu, original, approach. In this experiment, both approaches were applied to the pavement images from area scan camera.

Two steps from the original approach, grid cell analysis and crack seed verification, were reconstructed and applied to the pavement images so as to extract crack area. The approach started with choosing the pixels which were regarded as a

crack seed by using grid cell analysis in the first step. Then the crack seed was verified by using the contrast of a crack seed to their neighbors in the later step.

Similarity, two steps of the proposed crack segmentation phase, grid cell analysis chain and crack cell verification, were applied to the pavement images. The proposed approach enhanced grid cell analysis by decreasing the conditions that indicate the existence of crack, increasing areas of search and checking dark pixels arranging in the grid cell.

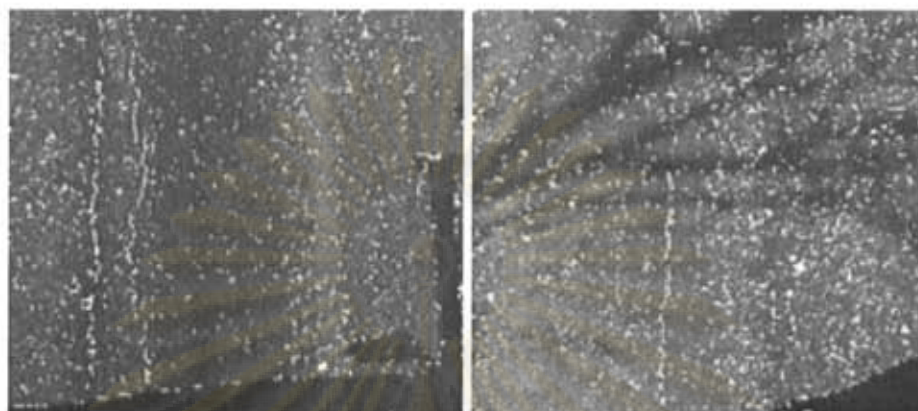
The sample pavement images in the experiment possessed different pavement textures and different light conditions. Some images had different brightness and some had low contrast. Both algorithms were applied with the constant parameters to those images. The results were shown in the following section.

### Experimental Results

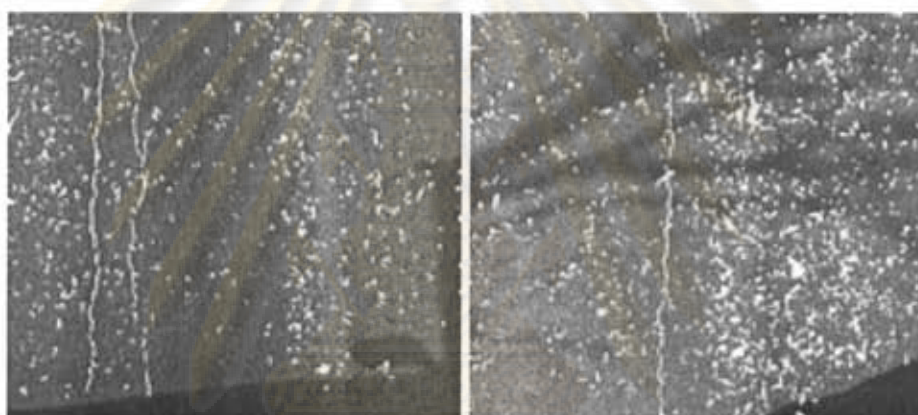
By applying original grid cell analysis approach [3] to sample images, the result images are shown in Figure 4.6(a). There was much noise appearing in the result images from strong texture and shadow problems. After applying the first technique, grid cell analysis chain, to the sample images, the noise from the shadow disappeared while the noise from strong texture were still in the result images as shown in Figure 4.6 (b). Finally, both techniques were applied to the sample images. From the result images shown in Figure 4.6 (c), this approach could extract most cracks from the sample images and also gave result with less noise.

Compared to the original algorithm, the proposed approach, using enhanced features, is less sensitive to light condition. Figure 4.7(a) shows the result images implemented with this approach. Figure 4.7(b) shows the result images implemented with the original algorithm. Both algorithms were applied to the same set of images with the same parameters, i.e. threshold values for original algorithm and window size for the proposed algorithm, for every single image. The results got from the proposed algorithm were satisfactory, while another gives best result only in the first image of Figure 4.7(b1).

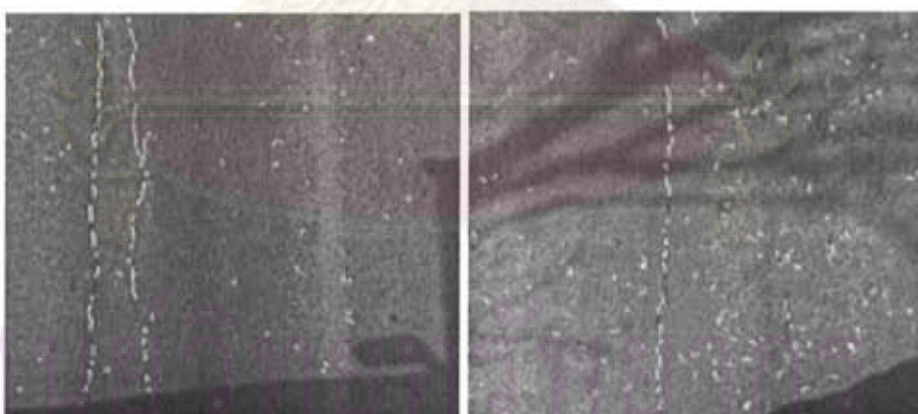




(a) GCA without Approached Techniques



(b) Applied Grid Cell Analysis Chain



(c) Applied Grid Cell Analysis Chain and Crack Cell Verification

Figure 4.6 Examples of Result Images

จุฬาลงกรณ์มหาวิทยาลัย



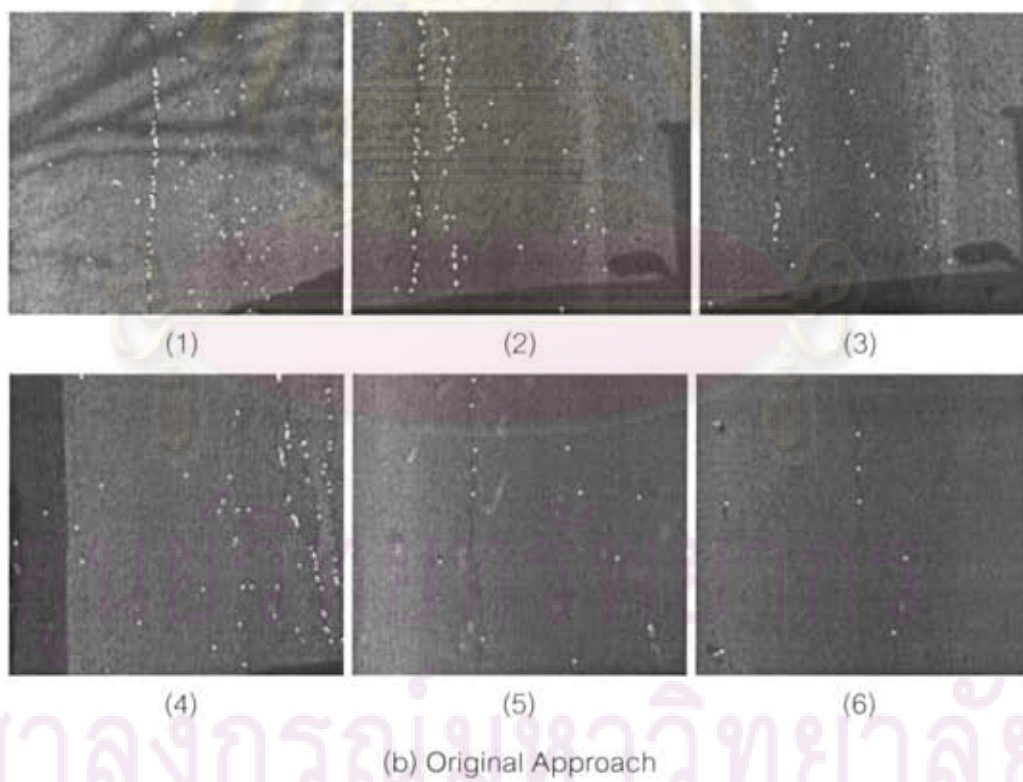
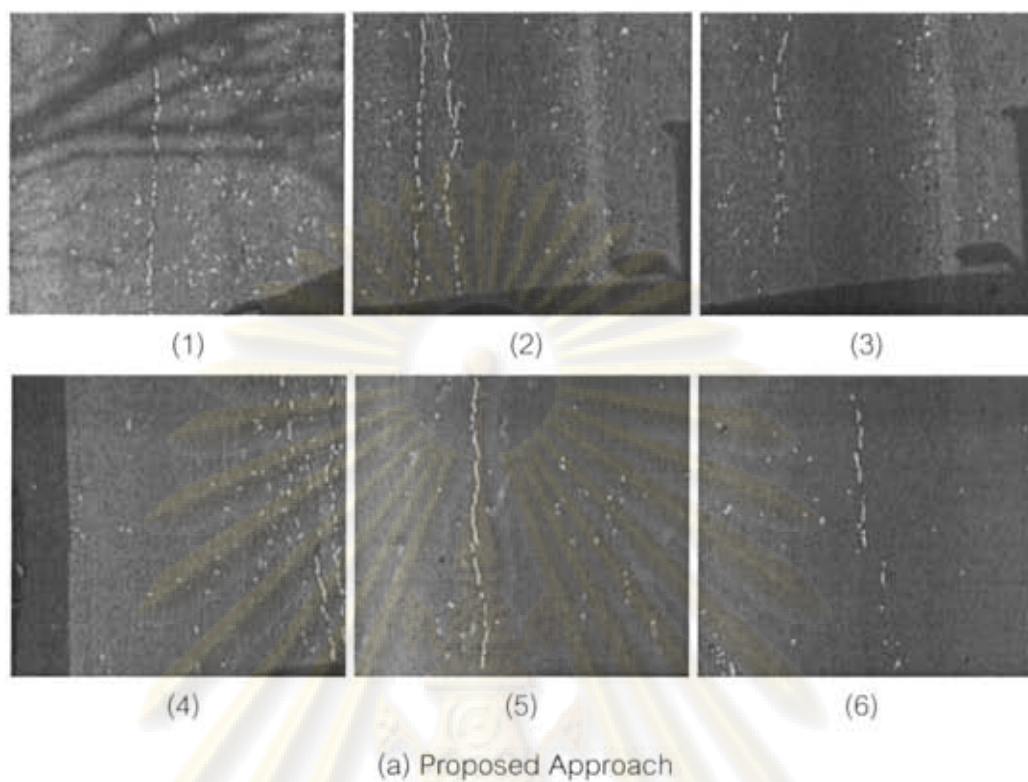


Figure 4.7 Experimental Result Images

Compared with Original Algorithm with Same Variable Values

#### 4.4 Noise Removal Experiment

The main distinguishing feature of crack objects from noise was the gravitation force feature which imitated the idea of natural phenomenon. This experiment was done in order to be evidence for the ability of the feature. The idea was implemented to the result images from crack segmentation phase.

The output images from crack segmentation phase were binary images. Crack objects, along with noise objects, were presented as white elements while the background was black. Object characteristics were extracted using convex hull technique [11]. The area and two tip positions of the objects were considered. Gravitation force feature of each pair of objects were calculated and investigated, (as shown in the pseudo code in Figure 3.13).

##### Experimental Results

To demonstrate the capability of this feature, the concept was applied to an example image to show the feature value. Figure 4.8 shows an example of noisy image. Considering object (0) in Figure 4.8, it is on a crack line with an area of 301 pixels. The other significant object information is shown in Table 4.1 with their feature values arranged in descending order.

The object (1) is on the same crack line as the considered object (0). Moreover, the object (1) is the closest object to the object (0). Unlike object (1), the object (2) is smaller and farther than the object (1). As a result, object (1) gives a feature value of 1,207.54 which is the highest value of the gravitational force towards object (0) while the object (2) gives 147.63 which is much smaller value.

Looking at object (3) in the Figure 4.8, it is the biggest object but very far away from the considered object (0). Consequently, it gives 16.85 which is a small amount of feature value or the gravitational force feature value.

Figure 4.9 shows the object where the considered object (0) is noise object with an area of 61 pixels. Significant object information is shown in Table 4.2. Since the considered object (0) is small, the biggest object gives small feature value, 4.46, compared to feature value of the object (1), 1,207.54, in Figure 4.8.



Figure 4.8 Considered Object (0) on a Crack Line

Table 4.1 Object Information for Figure 4.8

Interacting Object Number	Area (pixel)	Distance (pixel)	Gravitational Force (Feature Value)
(1)	682.00	13.04	1,207.54
(2)	489.00	31.58	147.63
(3)	1,444.00	160.59	16.85
(4)	277.50	87.86	10.82
(5)	469.50	160.00	5.52
(6)	12.50	27.89	4.84
(7)	40.00	52.09	4.44
(8)	1,191.00	436.15	1.88
(9)	1,277.00	479.76	1.67
(10)	136.00	168.24	1.45
(11)	786.50	457.56	1.13
(12)	63.00	130.98	1.11
(13)	163.00	212.05	1.09
(14)	77.50	149.60	1.04



Figure 4.9 Considered Noise Object (0)

Table 4.2 Object Information for Figure 4.9

Interacting Object Number	Area (pixel)	Distance (pixel)	Gravitational Force (Feature Value)
(1)	1,444.00	141.17	4.46
(2)	32.50	37.01	1.46
(3)	16.00	30.87	1.03
(4)	24.50	39.56	0.96
(5)	277.50	134.54	0.94
(6)	489.00	221.37	0.61
(7)	166.00	131.03	0.59



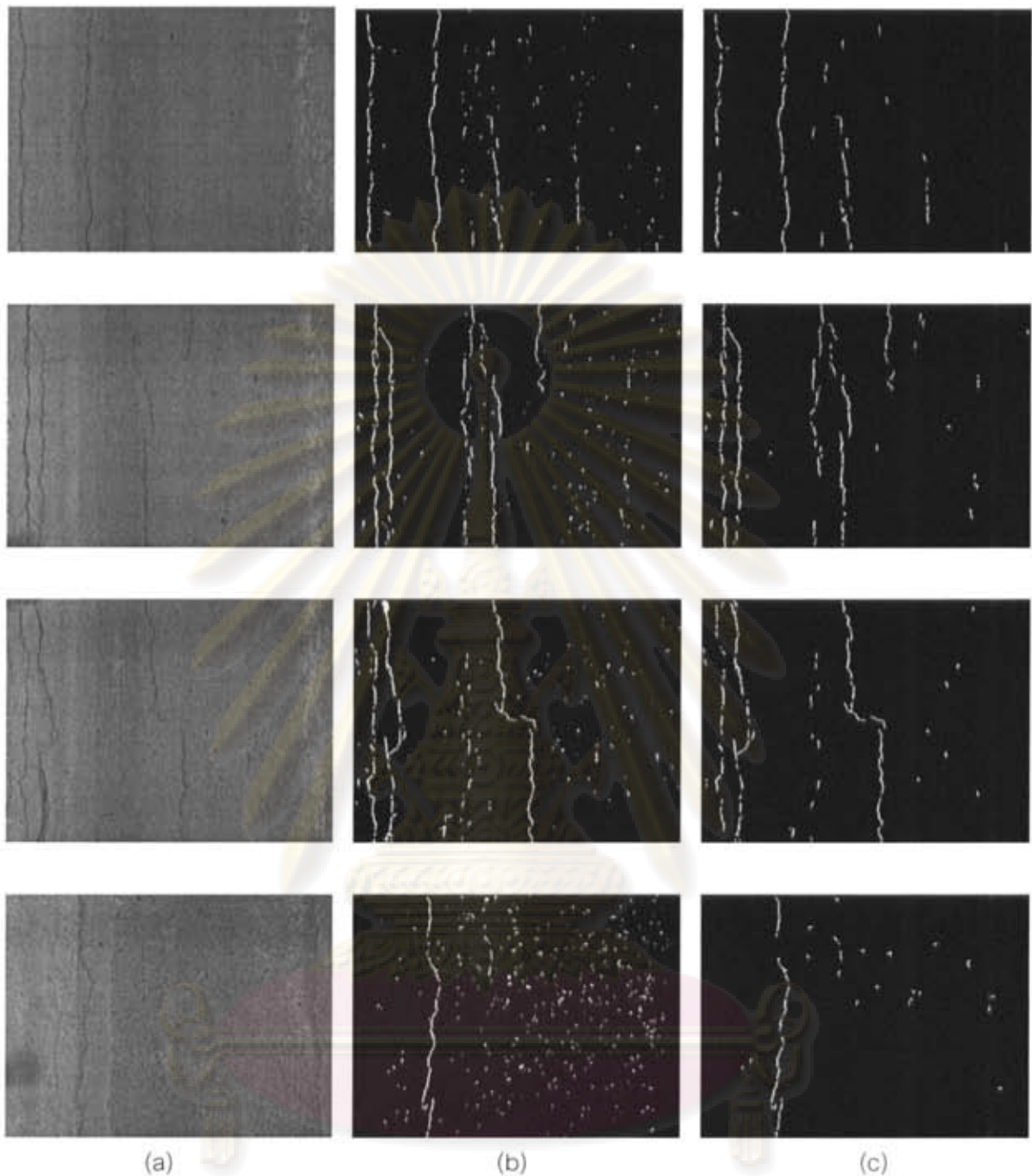


Figure 4.10 Noise Removal Result Images

Due to a high range of the feature value, the feature value then has the ability to distinguish an object as a noise or a crack. This feature was applied to the example images in Figure 4.10. Figure 4.10 column (a) shows the original pavement surface with the crack lines. Figure 4.10 column (b) shows the result image with many noise objects from crack detection algorithm. After applying this feature to remove noise, the clear crack lines appear. The results are shown in Figure 4.10 column (c).

#### 4.5 Measuring Accuracy

The proposed algorithm was applied to images from different roads with, different pavement textures, and different illumination conditions. The experiment can be viewed as two parts, the experiment with controlled input images and the experiment with real situation input images.

Experiment with controlled input images was done in order to measure the proposed approach accuracy under the research scope. The input images were manually selected to meet the research constraints. Then the selected input images were processed by the proposed algorithm. Finally, the output images, containing highlighted pixels, were carefully monitored and checked for the correctness of crack areas and positions by inspectors.

For the purpose of usability, the experiment with the real situation input images was done by embedding the algorithm in 'CU Crack Finder' program. The program handled the pavement input images in chronological order of the moving survey vehicle. The input images were fed into the algorithm, and then the output were stored in terms of bounded areas and types of crack. The bounded areas and types of crack were compared with the bounded areas and types of crack rated by human vision.

However, the reason that latter experiment was done was to test the algorithm with a large dataset of survey data where the input images could not be controlled. The input images included wet pavement roads, unpaved areas, or pavement shoulder covered with objects. During the survey, it was difficult to decide when to continue the survey after the rain. When the road surface of the earlier part of the road became dry, the later part may not be dry, or may be partially dry. This situation could cause the input images to be of mixed characteristics. It was impractical to wait until the wet surfaces were dry, came back to the same position to capture the dry pavement images. It was also difficult to avoid capturing the pavement images with unpaved shoulder.

Moreover, since the system could not perfectly taken all images with correct exposure, some images could be overexposed, underexposure, or contained lots of noise. For the above reasons, the latter experiment could give only partial useful accuracy but not all.

The accuracy of the experiments was measured in terms of false positive and false negative. False positive was wrong result from the algorithm on clean input images. False negative occur when the algorithm fail to detect cracks on distress input images.

#### 4.5.1 Measuring Accuracy with Controlled Input Images

In order to measure the accuracy, the proposed approach was applied to 3,991 images taken from different environment including strong texture and shadow. In this experiment, input images were chosen according to the scope of this research to measure the ability of the algorithm. The images were of dry asphaltic concrete road surface and did not include images of roads which were covered with objects, underexposed or overexposed.

The input images also contained other types of distress, e.g. raveling and poor patching area which gave strong texture images. Furthermore, the input images possessed poor illumination conditions which gave low contrast. Examples of the input images are shown in Figure 4.11.

Input images were classified by human inspectors into two categories, i.e. crack images and non-crack images. The experiment used grid cell size of 9x9 to find crack size of 5 mm. In order to classify the crack type, criteria used are shown below.

1. Crack area must be greater than 100 pixels or 3.24 square centimeters
2. If bounded area of a crack is more than 100 pixels or 18 centimeters in width and height, the crack will be judged as interconnected crack.
3. If bounded area of a crack is more than 100 pixels or 18 centimeters in width or height, the crack will be judged as linear crack.
4. Otherwise, a crack will be judged to be noise.

The results of the proposed algorithm with controlled input images are shown in Table 4.3. The approach gave an average of 3.07% false positive and 9.17% false negative.



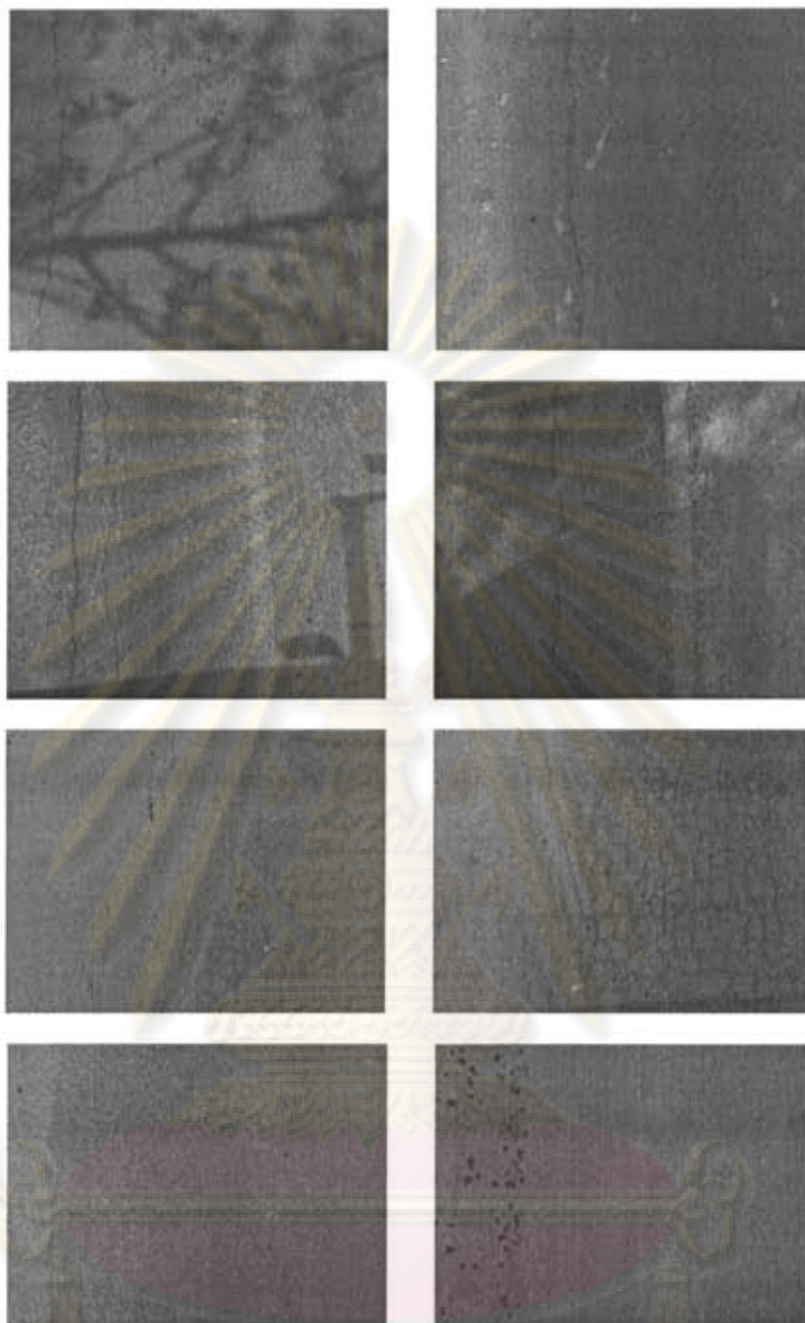


Figure 4.11 Examples of Input Images for Measuring Accuracy

Table 4.3 Results of Measuring the Proposed Approach Accuracy with Controlled Input Images

	Total	Correct	Incorrect
Non-Crack Distress Images	2,901	2,812	89
		96.93%	3.07%
Crack Distress Images	1,090	990	100
		90.83%	9.17%



#### 4.5.2 Measuring Accuracy with Mixed-characteristic Images from Real Survey

In this measurement, the proposed approach had been embedded as automatic distressed rating part in 'CU Crack Finder' program so as to measure the accuracy. The image files from real highway survey were decompressed and processed by the proposed algorithm. The output from this part was compared to the output from manual distressed rating part performing by inspectors.

The test data images were collected from three different routes in Loei province in June 2007. There were 75,926 pavement image frames. Each frame consisted of two pavement images which were stitched into one image. The images could be categorized into two types, clean pavement and distressed pavement. The distress can be classified as linear crack, interconnected crack, patching, pothole and raveling. The examples of input images are shown in Figure 4.12 and the total numbers of each distress type are shown in Table 4.4.

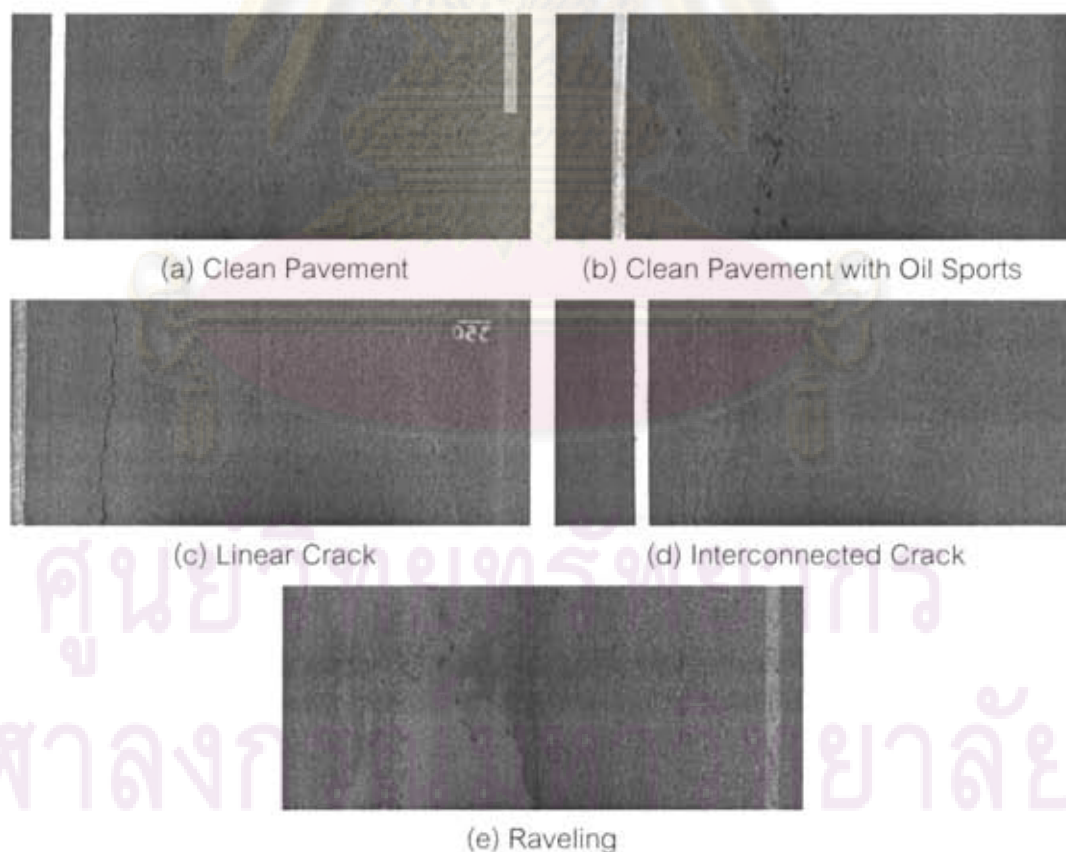


Figure 4.12 Examples of Input Pavement Images

Table 4.4 The Total Numbers of Each Distress Type

	Number of Image Frames	Distance (km.)	Frames with Distress				
			Interconnected Crack	Linear Crack	Patching	Pothole	Raveling
Route 1	41,365	72.39	3,832	1,774	1,271	792	4,155
Route 2	21,153	37.02	936	112	1,077	594	3,000
Route 3	13,408	23.46	407	939	390	309	874
Sum	75,926	132.87	5,175	2,825	2,738	1,695	8,029

Because this research focused on crack distress only, other distress, such as patching, pothole and raveling were summed up as other types of distress. However, an image might contain more than one type of distress. For example, crack distress may appear near/or in the same area as raveling. Figure 4.13 shows such example. In Figure 4.13(a), raveling distress is scattered over the image, but there is a crack line on the top left of the image, which does not appear on the raveling area. In this case, the inspector marked the crack as linear crack, and marks the raveling area as raveling area. Unlike Figure 4.13(a), there is a crack line on raveling area in Figure 4.13(b). In this case, the

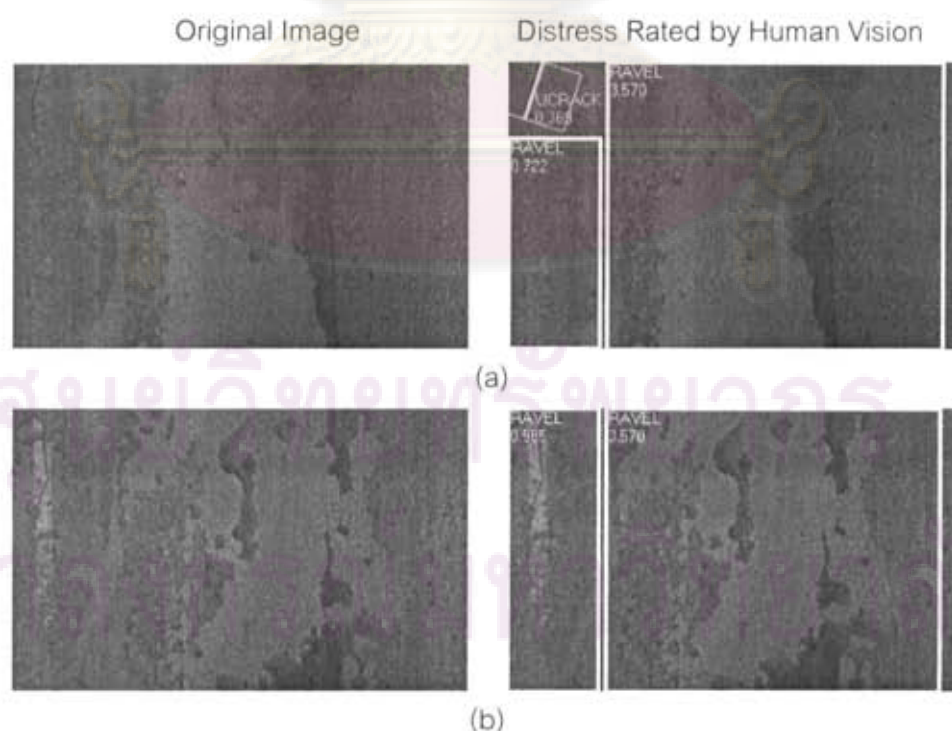


Figure 4.13 Examples of Two Type of Distress in an Image

inspector chose the most severe distress, which was raveling distress. Therefore the crack line was not labeled. The total numbers of distressed image frames that consist of more than two types of distress in different area are shown in Table 4.5 and Figure 4.14.

Table 4.5 The Total Number of Distressed Image Frames

Distress Types Appearing in an Image	Total Number of Image Frames			
	Route 1	Route 2	Route 3	Sum
Crack Distress Only (Unidentified Type)	5,488	1,031	1,302	7,821
Crack Distress with Other Types of Distress	1,220	372	202	1,794
Interconnected Crack and Linear Crack	118	17	44	179
Interconnected Crack and Other Types of Distress	1,053	360	87	1,500
Linear Crack and Other Types of Distress	202	17	131	350
Interconnected Crack, Linear Crack and Other Types of Distress	35	5	16	56

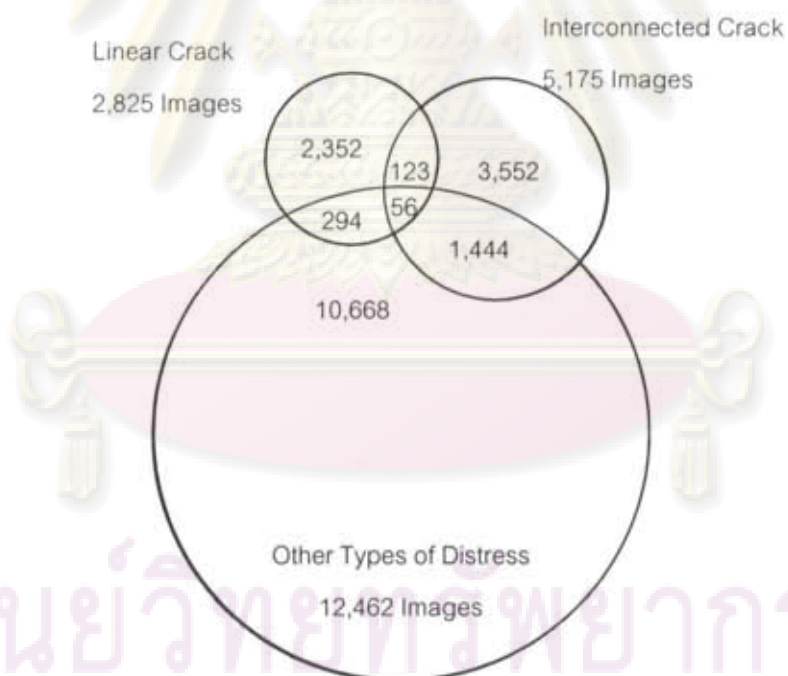


Figure 4.14 Venn Diagram of Distress Image Frames

In manual distress rating part, the area of distress appearing in pavement view images were bounded by non-rotate rectangles or lines depending on the type of distress. In automatic distressed rating part, crack distress was located, classified and



measured by crack detection algorithm using image processing techniques. The results from the automatic part were the bounded area represented by rectangles which were rotated to fit the minimum crack area. The examples of rating are shown in Figure 4.15.

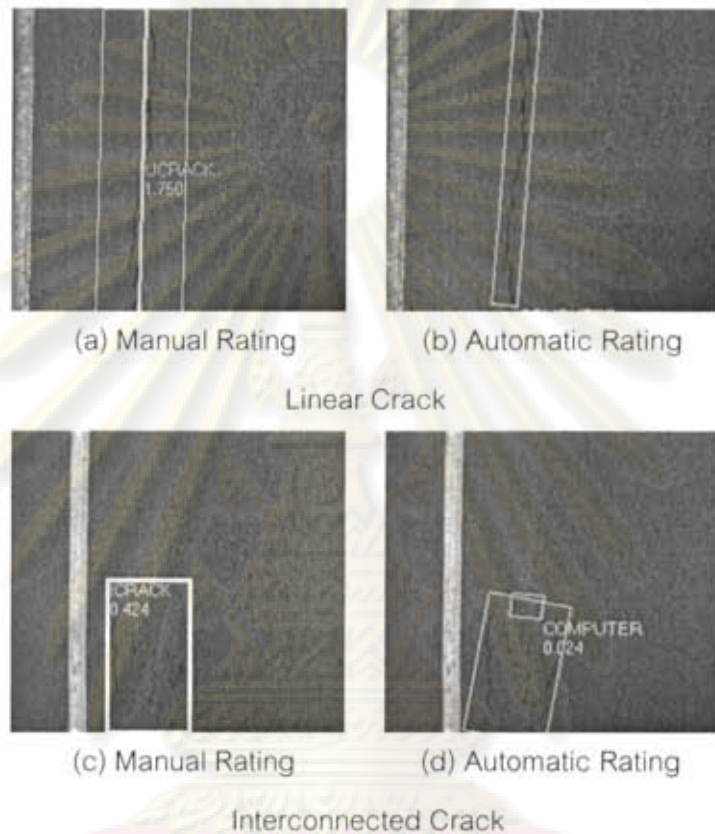


Figure 4.15 Manual and Automatic Distress Rating

Because of some different criteria used by human rating and automatic rating, it is difficult to compare the area of crack to conclude for accuracy. Rating by human vision was subjective, estimated, and might not fit with the real crack whereas rating by algorithm attempted to fit the real crack and excluded unwanted areas. In order to check the correctness, the locations of cracks in an image were estimated and compared.

This experiment also used grid cell size of 9x9 to find crack size of about 5 mm similar to the controlled input case in section 4.5.1. The results are shown in Table 4.6. The approach gave an average of 6.20% false positive and 46.99% false negative,



where 38.20% in 46.99% were from images of pavement conditions outside the research scope.

Table 4.6 Results of Measuring the Proposed Approach Accuracy with Mixed-Characteristic Input Images

	Total	Correct	Incorrect
Non-Crack Distress Images	143,852	134,929	8,923
		93.80%	6.20%
Crack Distress Images	8,000	4,241	3759*
		53.01%	46.99%*

Remarks: 3056 images (38.20%) were of wet pavement and/or images not in the scope of this research

### 4.5.3 False Positive

False positive is the wrong result from the algorithm on clean input images. Crack area should not be found when applying the algorithm on clean input images. The cracks which were detected on these images was called false positive. The causes of false positive are show in the following sections.

#### 4.5.3.1 Oil Stains

False positive might be caused by several reasons. Oil spots on pavement road were an example. The round shape oil spot was easy to distinguish from crack lines, whereas the oil stains of line shape also had same characteristics as crack lines. Consequently, the proposed approach could handle the oil spots in round shape, but give the false positive on images with oil stains of line shape, as shown in Figure 4.16.

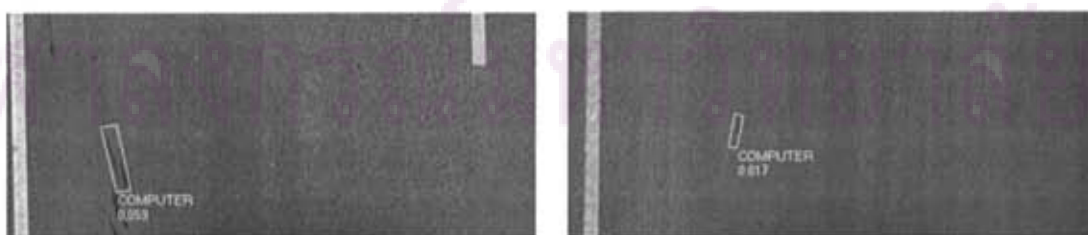


Figure 4.16 False Positive on the Images with Oil Lines

### 4.5.3.2 Objects on Road Pavement

In the survey, the roads were not always clean. Some areas were covered with dirt or soil which came from factories located nearby or fell from trucks. Because the contrast and shape were the main considered factors to define crack characteristics, these dirt or soil could form texture similar to crack lines and might cause false positive. The examples of this kind of false positives are shown in Figure 4.17(a). The Figure 4.17(a) shows an image of pavement covered with white dust forming shapes like crack lines. This situation occurred when a wheel tire ran over white dust and created tire track on the pavement surface. The tire tread portion that did not pick up the dust might cause a crack-like line. Consequently, the algorithm evaluated this line as a crack line.

Because road shoulders might appear in the input images, objects that were not part of the road, e.g. grass, hay or tree branches could show up in the images. Figure 4.17(b) shows an image with hay on the shoulder area which was judged to be crack area.



Figure 4.17 False Positive on the images with objects

### 4.5.3.3 Strong Texture and Illumination Problems

The proposed algorithm was designed to cope with illumination and strong texture problems. The algorithm tended to give a good result with non-uniform illumination image but it still gave false positive area in some strong texture images. Figure 4.18 shows example images of this case.

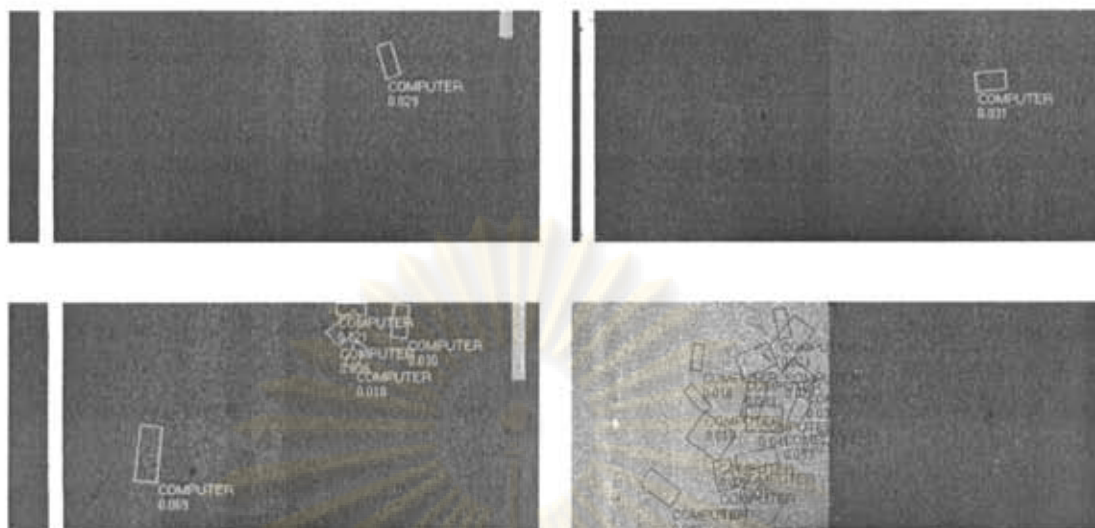


Figure 4.18 False Positive on the Images with Strong Texture and Illumination Problems

#### 4.5.3.4 Wet and Noisy Images

Because of long distance of the survey, it was difficult to select the input images according to the research scope. Wet surfaces were one of the uncontrolled factors, as shown in Figure 4.19, which might give false positive. However, not only wet surfaces, noisy images also gave the false positive error. Figure 4.20 shows an example of noisy image with false positive error.

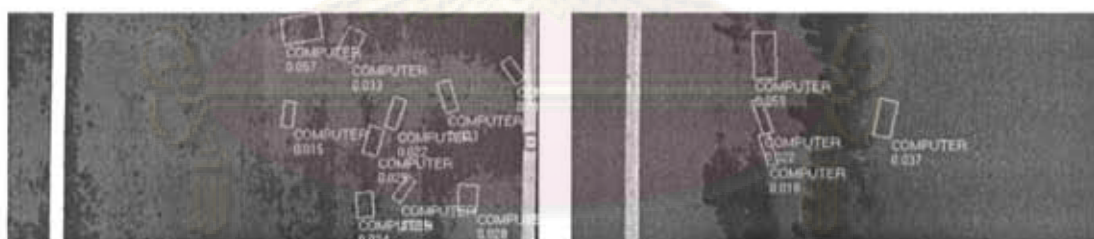


Figure 4.19 False Positive on the Wet Pavement Images



Figure 4.20 False Positive on Noisy Image



#### 4.5.3.5 Other Types of Distress

Another uncontrolled factor was the crack distress that might be mixed with other types of distress. In this case, the human rater picked the most severe one or a better representative one to represent part of the pavement that was needed to be repaired. The examples of this case are shown in Figure 4.21. There were interconnected crack beside the patching area in Figure 4.21 (a). In this case, the inspector marked the distress as patching area and ignored the crack area. On the other hand, the algorithm did not have any knowledge about patching. It did not realize that patching and crack were together. Consequently, the crack was found and marked by the algorithm.

Similarly, Figure 4.21 (b) shows a crack on an area that was judged by the rater to be a raveling area. After applying the algorithm to the image, the crack line was marked. The correctness was measured by comparing crack positions that were defined by human vision to those defined by the algorithm. Such situation caused false positive error even if the algorithm could indicate the cracks.

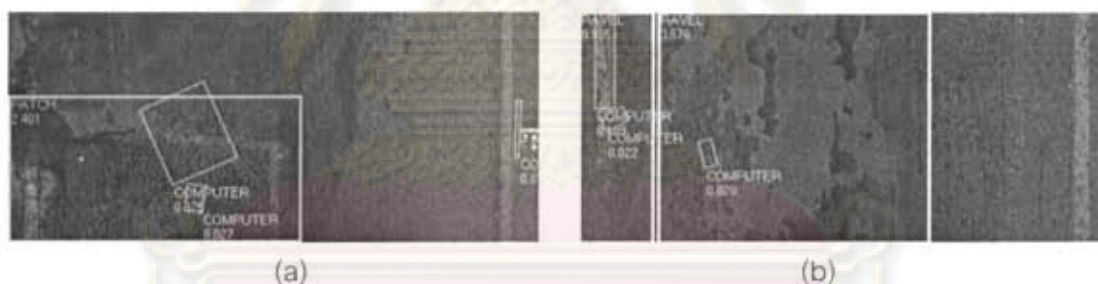


Figure 4.21 False Positive on Crack and Other Types of Distresses

In some cases, false positive occurred when there were other types of distress or patching in the input images. Examples of these cases are shown in Figure 4.22. These patching or raveling areas had different characteristics from clean pavement. The algorithm, sometime, found them as crack areas which were judged as false positive error. The majority of these false positive cases was raveling distress as shown in Table 4.7 and Figure 4.23.



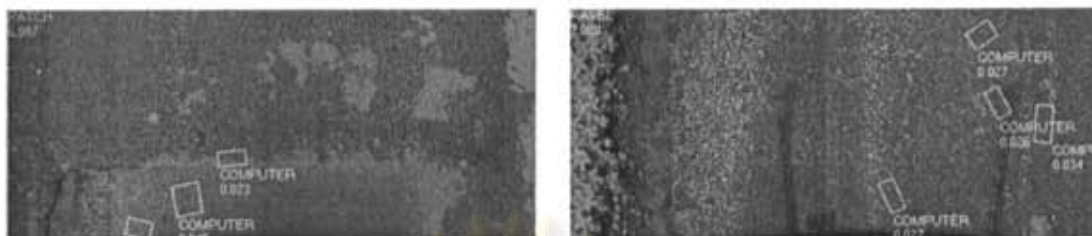


Figure 4.22 False Positive on Distressed Images.

Table 4.7 Total Number of Distressed Images with False Positive Error

Distress Type	Crack Distressed Images Judged by the Algorithm	
	Images	Percentage
Pothole	1,084	12.26%
Patching	1,897	21.45%
Raveling	5,862	66.29%

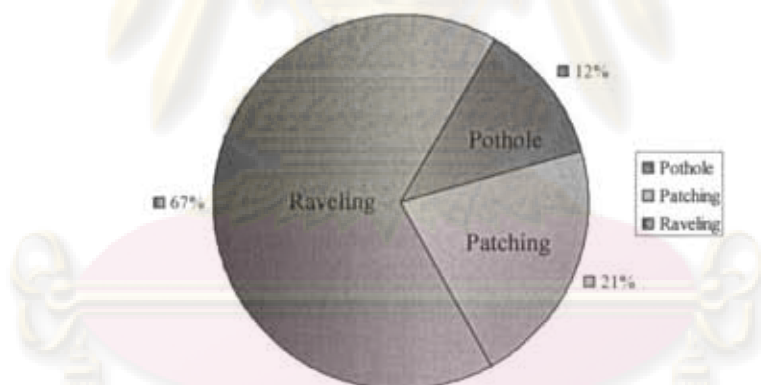


Figure 4.23 Total Number of Distressed Image with False Positive Error

#### 4.5.4 False Negative

In contrast to false positive, false negative is the measure of the fault that occurs when the algorithm cannot detect crack which appears on an input image. The causes of the false negative are described in the following sections.

#### 4.5.4.1 Causes of False Negative in the Controlled Input Images

Investigating into the 9.17% false negatives in the controlled input images, most cases were found in the crack identification phase. Because only some parts of the crack lines could be extracted, small pieces of crack object could not be merged. From this reason, the crack characteristics cannot be derived, so the crack area was not found. Example images of this problem are shown in Figure 4.24.

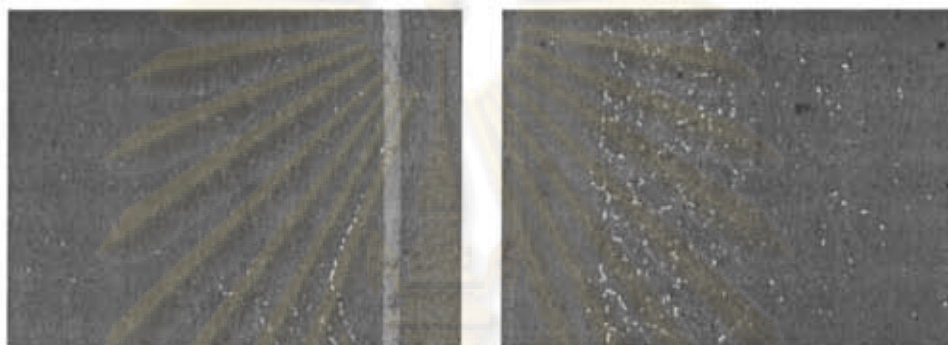


Figure 4.24 False Negative on Controlled Input Images

#### 4.5.4.2 Cause of False Negative in the Mixed-Characteristic Input Images

From the investigation, the causes of false negatives occurred came from the following factors.

1. Human fault.
2. Larger crack size (compared to grid cell size).
3. Thin crack.
4. Noise in the input images.
5. Low contrast of the input images.

##### 1) Human Fault

Practically, manual distressed rating may not be 100% reliable. 'CU Crack Finder' helps inspector to speed up the marking of distressed areas by integrating pavement images into one image. The inspector marked distressed areas on the

merged images without knowledge about separated images. Because of enormous amount of data being rated, sometime the rater marked distressed areas more than reality which might cause false negatives.

Figure 4.25 shows an example of linear crack rating. The upper image did not contain any cracks while the lower image contained a crack line. The rater sometime estimated the length of crack line incorrectly by dragging the pointing device too far causing the length of the crack to occupy two images as shown in Figure 4.25(c). The algorithm found only crack lines on the lower image as shown in Figure 4.25(b). Therefore, the comparison gave false negative error on the upper images.

In some interconnected crack distressed images, as shown in Figure 4.26, the rater also estimated distressed area which over occupies two images. Figure 4.26(a)

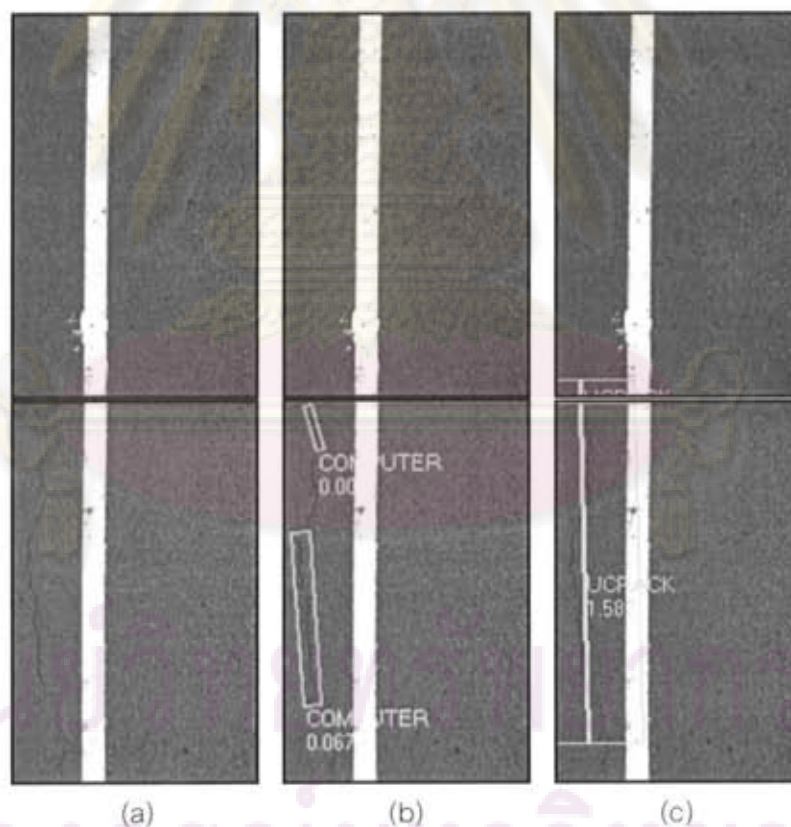


Figure 4.25 Linear Crack Rating

(a) Original Images

(b) Rating by Algorithm

(c) Rating by Human Inspector

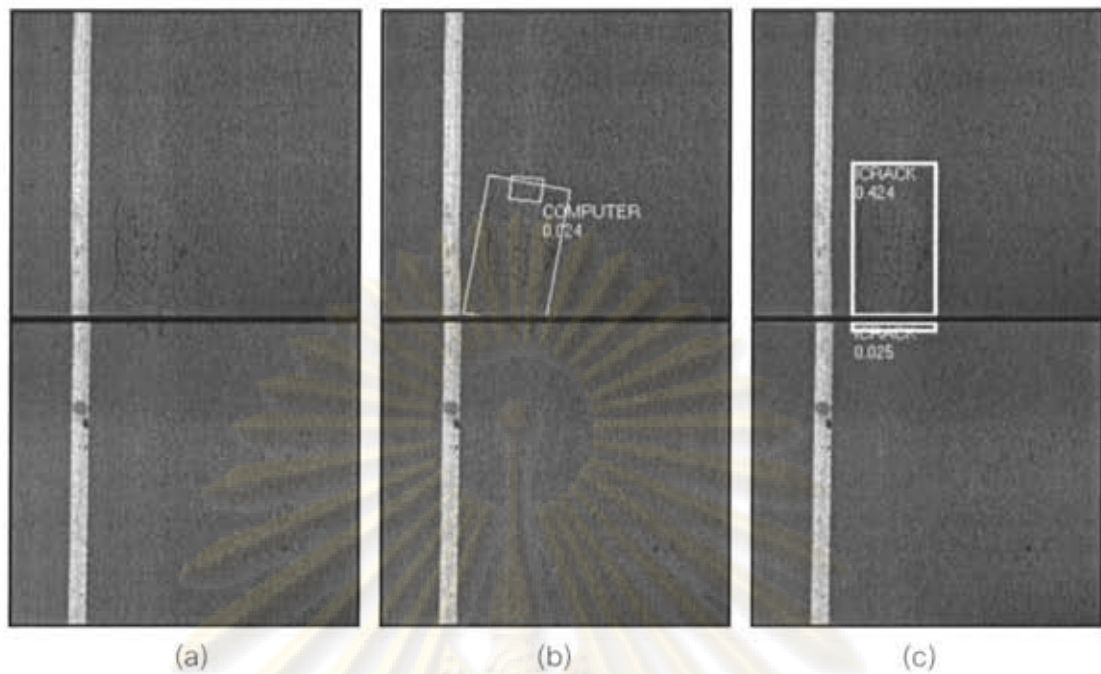


Figure 4.26 Interconnected Crack Rating

- (a) Original Images
- (b) Rating by Algorithm
- (c) Rating by Human Inspector

shows the original images with interconnected crack on the upper image. Figure 4.26(b) shows the images with crack bounded area by the algorithm. Only interconnected area on the upper image was found. Figure 4.26(c) shows the images with crack bounded area by human vision. The bounded area of interconnected crack occupied both images which gave false negative error on the lower image.

In order to show several pavement frames on the screen, the pavement images were resized. The rater might not clearly judge the images, so the rater might make a mistake. For example, Figure 4.27 shows examples of sealed cracks images which inspector rated as linear crack. In this case, the algorithm did not find the crack. Consequently, the comparison gave false negative.



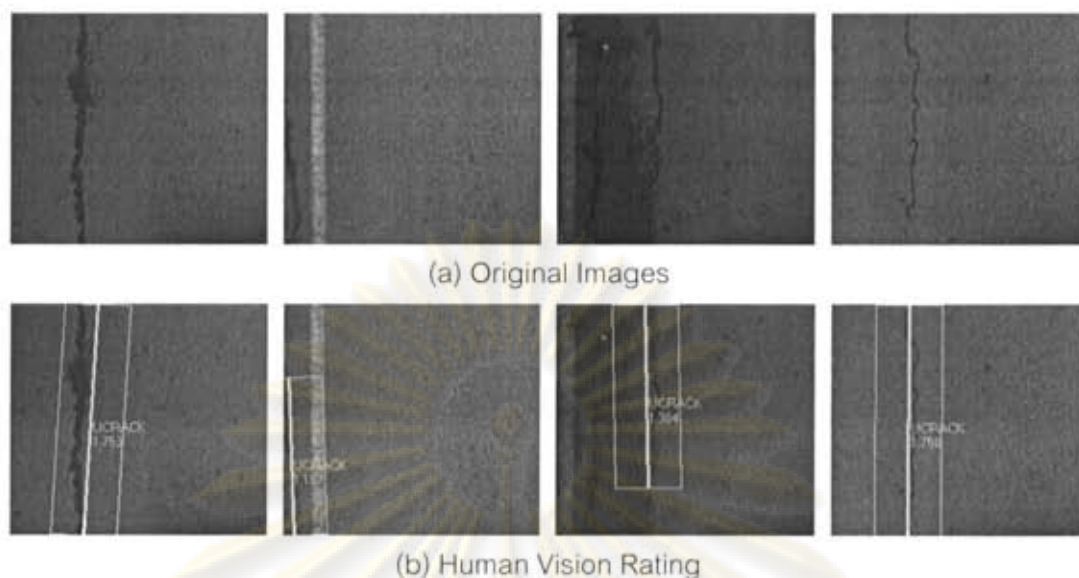


Figure 4.27 Rating with Wrong Type of Distress

## 2) Larger Crack Size (Compared to Grid Cell Size)

Because the pavement might not be absolutely dry during the survey, the crack distress might absorb water on the surface, causing thick lines along the crack. These thick lines were one of the inevitable consequences. Since the proposed algorithm was effective in detecting cracks within a range of crack width, the cracks with water absorbed tended to give a look-alike thick crack lines. As a result, such cracks could not be detected. Examples of larger crack size are shown in Figure 4.28.

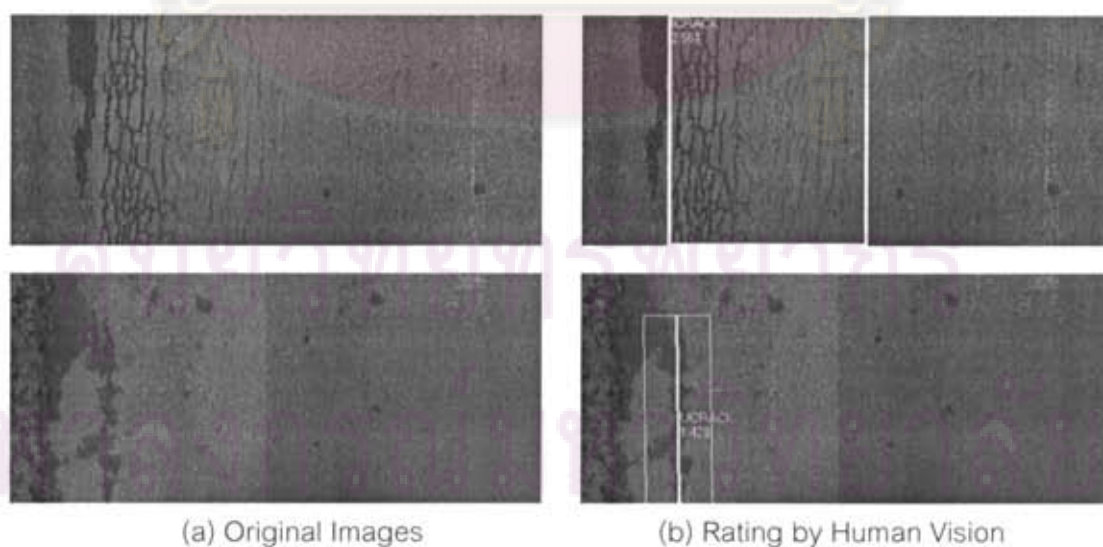
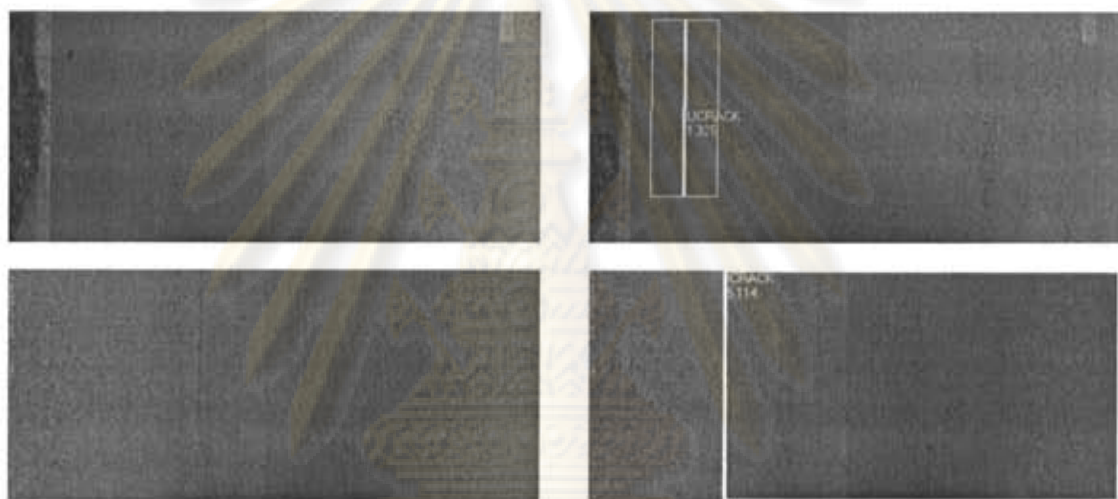


Figure 4.28 Examples of Larger Crack Size

### 3) Thin Crack

In the rating process, the inspector marked crack distress areas if they are visible on the images without considering the crack sizes. In many cases, some cracks appear on the images as one-pixel crack width. The inspector could recognize them and mark the area of crack distress. However, the algorithm could detect only cracks around five millimeters of width which appeared on the image about three-pixel width. Therefore, the one-pixel crack was ignored by the algorithm, causing the false negative error.



(a) Original Images

(b) Rating by Human Vision

Figure 4.29 Examples of Smaller Size of Cracks

### 4) Noise in the Input Images

Since the sunlight during the survey was not uniform through out the day, it sometime became darker because of shadow from cloud, trees, or buildings. This situation might cause noisy images, as shown in Figure 4.30. The image with a lot of noise might not be a problem with human vision but it could cause false negative error to the algorithm.

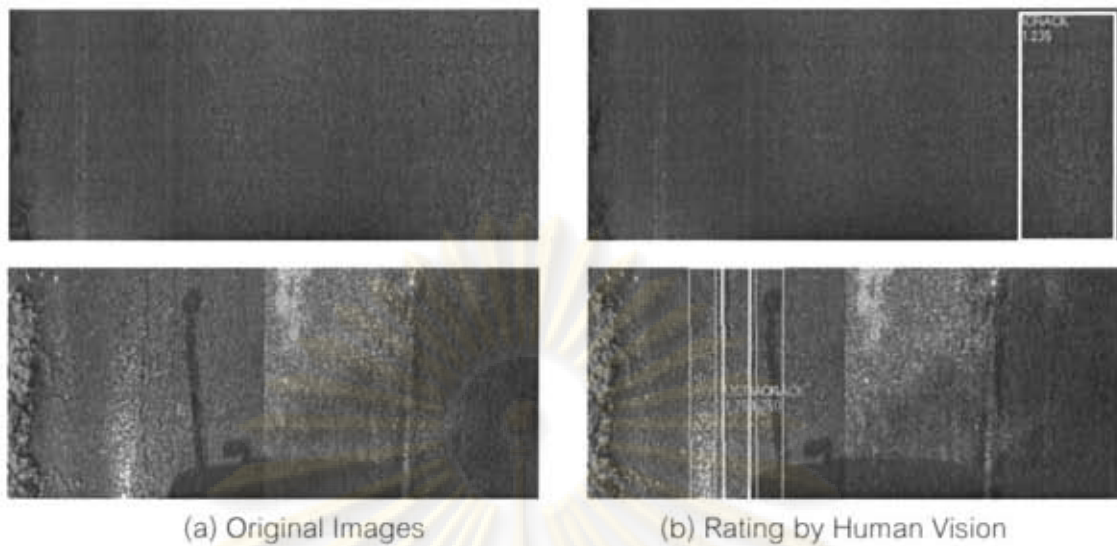


Figure 4.30 Noisy Input Images

#### 5) Low Contrast Input Images

The proposed algorithm was developed based on the assumption that a crack line is a narrow strip of pixels whose intensity is perceptible darker than the surrounding background. Most crack characteristics depend on contrast of crack and the background. In the low contrast images, crack lines are difficult to be noticed. Therefore, it was hard to define low contrast cracks by the algorithm. The examples of low contrast images are shown in Figure 4.31.

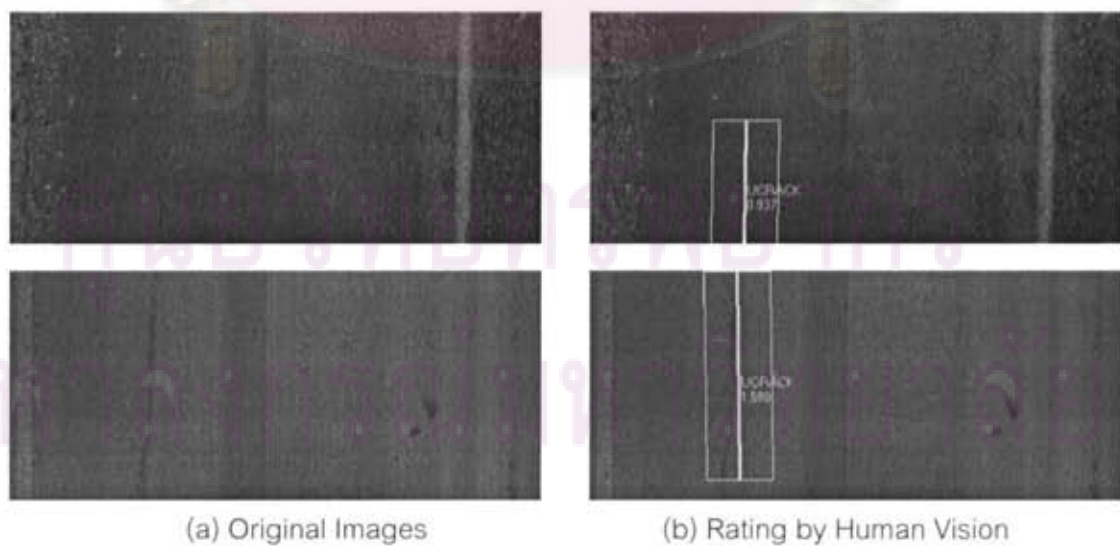


Figure 4.31 Low Contrast Images



#### 4.5.4.3 Investigating of False Negative on the Mixed-Characteristic Input Images

False negatives in the mixed-characteristic input images were investigated so as to find the causes. Due to the vast amount of survey images, the input images were sampled every 100 meters for the investigation. The samples showed that 80.31% of false negatives were caused by wet and low contrast images which were not in the research scope. After excluding these out-of-research-scope crack images, the false negative is about 14.822% as shown in the Table 4.8.

Table 4.8 Mixed-characteristic Input Images after Ignoring out of Scope Input Images

	Total Crack Distress Input Images		Excluding Out-of- Scope Crack Images	
	Total	8,000	100.00%	4,944
Correct	4,241	53.01%	4,241	85.78%
False Negative	3,759	46.99%	703	14.22%
In Scope	703	8.79%		
Out of Scope	3,056	38.20%		

False negative images were investigated and can be classified as classification fault and crack detection fault. The total number of false negative images is shown in Table 4.9.

Table 4.9 Causes of False Negative in Mixed-Characteristic Input Images

	False Negative Images	
	Classification Fault	238
Crack Detection Fault	465	9.41%
Sum	703	14.22%



Crack type classification fault was one of the false negative causes. Although crack identification phase needed knowledge from a professional inspector, crack identification by human rater team was subjective. Because of the different knowledge background, wrong classification might occur in some situations. The example images of classification fault are show in Figure 4.32.

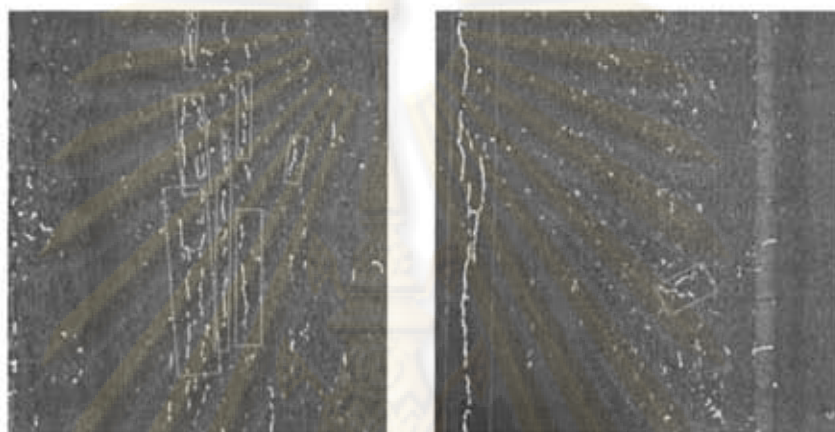


Figure 4.32 Examples of Classification Fault

Another false negative cause was crack detection fault where crack line was not detected. Causes of crack detection fault with total number of images are shown in Table 4.10. The explanations for the caused were already described in prior sections.

Table 4.10 Causes of Crack Detection Fault

	Total Images	
	Gradient crack	257
Thin crack	154	3.11%
Crack cells found but too scatter and cannot be grouped as cracks	54	1.09%
Sum	465	9.41%

## CHAPTER V

### CONCLUSIONS AND RECOMMENDATIONS

This chapter draws conclusions of the research and also includes comments and recommendations of the algorithm for real situations.

#### 5.1 Conclusions

This research was to develop an algorithm to detect crack in asphaltic concrete road surface images using enhance grid cell analysis. The algorithm was tested with pavement images in 8-bit gray-level MJPG format with ground resolution of approximately 1.8 mm/pixel. With intention to find 5 millimeters cracks which appears in an image as crack lines with 3 pixels strip width, grid cell size used in this research crack was 9x9 pixels. The image processing ran on an Intel Centrino Duo 2.16 GHz computer with 1GB RAM. The conclusions of the research are as follows.

1. The algorithm was divided into four phases. The first phase, called the pre-processing phase, helped enhance the original images. The second phase was the crack segmentation phase which extracted crack objects from the output of the first phase. Next, the noise removal phase was used to reduce noise from the second phase. Finally, the crack identification phase was used for classifying crack types.

2. The pre-processing phase used morphological techniques to improve the input images. Opening and closing techniques were applied in order to make the crack lines become darker and eliminate dark spots.

3. The second phase, the crack segmentation phase, consisted of two parts. The first part was the grid cell analysis chain part which solves shadow and shading problems. This part reduced the number of conditions to indicate crack cell in order to reduce noise. It also increased the analyzing areas on an image by processing the image in an overlapping way. The second part was the crack cell verification phase

which used the assumption that all the crack cells should have crack pixel arrangement closed to the imaginary line. This feature significantly improved the accuracy in extracting crack lines on a pavement image with non-uniform illumination and strong texture.

4. The third phase was the noise removal phase. This phase introduced an image processing feature for noise removal in images from the second phase. Unlike other types of noise, noise of this kind was unique in terms of size and dispersal. The feature was based on the theory of universal gravitation. This feature was applied to objects for keeping crack objects separated from noise. After applying the feature to the noisy images, the crack lines were easier to be noticed.

5. The last phase of the proposed algorithm was the crack identification phase. In this phase, the crack objects from the third phase were grouped together using convex hull technique. Crack characteristics could be extracted and used to classify crack types. However, this phase needed knowledge from professional inspectors to define crack characteristics.

6. The accuracy of the proposed algorithm was measured by applying the algorithm to the input images which were manually selected according to the research scope. The measurement results with 3.07% false positive and 9.17% false negative. Images with oil stains are the main cause of false positive. False negative is caused by segmentation phase that can extract crack cell but too scatter to be grouped as crack.

7. In order to test the capability of the proposed method in real situation, the proposed approach was applied to pavement images from the survey in open environment. With the test dataset of 4944 frames of dry pavement containing cracks, false negative of 14.86% was achieved. With the data set of 70,000 frames, false positive of 6.2% was achieved. Images with oil stains, object, and other type of distress are the cause of false positive. False negative is caused by gradient cracks, classification fault and segmentation fault as described in previous section.



## 5.2 Contributions

This research can be applied to an automatic crack detection system in order to find crack size (bounded area) and its position within images with the performance of about 0.7 second processing time per frame when used with a computer as described earlier. Highway management system or systems that use similar result can benefit from reliable crack detection of this research. Automatic or semi-automatic crack detection can be used. In semi-automatic rating, a rater can skip non-crack pavement images and pay attention to the portion of the dataset containing cracks. Distress rating time can then be reduced, and reliable result within a range of accuracy can be achieved.

## 5.3 Limitations

This research was developed under constraints of most asphaltic concrete highway pavement conditions but might not be suitable for all cases. The limitations of this research are as follows.

1. The algorithm was proposed to detect crack lines which appear in the images as darker strip pixels. Other crack lines appearance, e.g. white crack lines, crack lines with lighter intensity than the background, gradient crack lines, crack lines with low contrast to the neighbouring background, may not be detected.
2. Since the proposed algorithm needs good contrast between crack lines and background, wet pavement image must not be used
3. The proposed algorithm was developed to detect most cracks on the highway pavement image dataset already on hand where a pixel represents about 1.8 millimeters of actual length and most crack line width was about five millimeters or three pixels. The algorithm gave good result when using a grid cell size of 9x9. Other configuration may not give the accuracy within the range of this research result.



4. In addition, crack characteristics were defined that crack area must be more than 100 pixels or 3.24 square centimetres, or 100 pixels or 18 centimetres in width or/and height. Otherwise, the objects detected would be judged as noise. Real use of this algorithm should follow these constraints.

#### 5.4 Comments and Recommendations

When applying the proposed algorithm to the real survey data, several issues should be considered. Also, improvement may be possible to cope with current limitations and to give better accuracy. These issues are described below.

1. In order to get the quality of the result as described in this research, survey should be done in sunny days. The pavement must be dry and the pavement should be cleared of hay, grass, or other objects that may cover the pavement.

2. In a situation where a route is not in the conditions mentioned above, the survey data should be viewed randomly by human to judge the quality of the input images. If the pavement images are mostly within the algorithm constraints, they shall be processed by the algorithm in order to find crack areas. Otherwise, the crack distress should be judged by human vision.

3. Changing grid cell size may help improve crack detection algorithm. Since crack lines that can be detected by the proposed algorithm depend on the grid cell size, a certain size of grid cell is good to detect only one size of crack width. As a result, using various sizes of grid cell may help to broaden the scope of crack detection.

## References

- [1] J. Pynn, A. Wright, and R. Lodge. Automatic identification of cracks in road surfaces. Seventh International Conference on Image Processing and Its Applications, Manchester, UK 1999 : 671-675.
- [2] I. Sokolic. Criteria to Evaluate the Quality of Pavement Camera Systems in Automated. Master of Science in Civil Engineering Department of Civil and Environmental Engineering College of Engineering University of South Florida, 2003.
- [3] B. Xu and Y. Huang. Automatic Inspection of Pavement Cracking Distress. Journal of Electronic Imaging 2006 : 5909.
- [4] S.-N. Yu, J.-H. Janga, and C.-S. Han. Auto inspection system using a mobile robot for detecting concrete cracks in a tunnel. Automation in Construction 2007 : 255-261.
- [5] M. Yan, S. Bo, K. Xu, and Y. He. Pavement Crack Detection and Analysis for High-grade Highway. The Eight International Conference on Electronic Measurement and Instruments 2007 : 4-548 - 4-552.
- [6] H. G. Zhang, and Q. Wang. Use of Artificial Living System for Pavement Distress Survey. Industrial Electronics Society, 2004. IECON 2004. 30th Annual Conference of IEEE 2004 : 2486- 2490.
- [7] T. Tomikawa. A study of road crack detection by the meta-genetic algorithm. AFRICON, 1999 IEEE 1999 : 543-548.
- [8] D. Meignen, M. Bernadet, and H. Briand. One Application of Neural Networks for Detection of Defects Using Video Data Bases: Identification of Road Distresses. Proceedings of the 8th International Workshop on Database and Expert Systems Applications 1997 : 459 - 464.
- [9] P. Subirats, J. Dumoulin, V. Legeay, and D. Barba. Automation of Pavement Surface Crack Detection using the Continuous Wavelet Transform. 2006 IEEE International Conference on Image Processing 2006 : 3037-3040.
- [10] H. Heijmans, "Mathematical Morphology and Image Processing," Online Document

URL: <http://www.ercim.org/publication/> 1999.

- [11] R. C. Gonzalez and R. E. Woods. Digital Image Processing. Prentice-Hall, 2002.
- [12] G. F. Luger. Artificial Intelligence: Structures and Strategies for Complex Problem Solving : Addison-Wesley, 2005
- [13] N. Drakos, Newton's Law of Gravity. Online Document URL: <http://theory.uwinnipeg.ca/>:1999
- [14] Full Report. A Study and Analysis of Road Distress Project in Northern Part of Thailand, Department of Highway, Ministry of Transport, and CERT, Department of Engineering, Chulalongkorn University, 2007



ศูนย์วิทยทรัพยากร  
จุฬาลงกรณ์มหาวิทยาลัย



ศูนย์วิทยทรัพยากร  
จุฬาลงกรณ์มหาวิทยาลัย



## Appendix A

### Experimental Results

This section shows the experimental results of applying the proposed algorithm to mixed-characteristic input images from real highway survey. The experiment used grid cell size of 9x9 to find crack size of 5 mm. In order to classify the crack type, criteria used are shown below.

1. Crack area must be greater than 100 pixels or 3.24 square centimeters
2. If bounded area of a crack is more than 100 pixels or 18 centimeters in width and height, the crack will be judged as interconnected crack.
3. If bounded area of a crack is more than 100 pixels or 18 centimeters in width or height, the crack will be judged as linear crack.
4. Otherwise, a crack will be judged to be noise.

The experiment was separated into two parts according to input images types. In the first part, the experiment measured accuracy of crack detection on clean input images. The measurement was shown in false positive. In the other part, the experiment measured accuracy of crack detection on crack input images. The measurement was shown in false negative.

ศูนย์วิจัยทรัพยากร  
จุฬาลงกรณ์มหาวิทยาลัย

Table A.1 False Positive in Mixed-Characteristic Input Images

Route	Type Image	Clean Images				
		Total	Crack Found (False Positive)		Crack Not Found (Correct)	
Route 1	Crack Distress	35,877	2,374	6.62%	33,503	93.38%
	Interconnected Crack	37,533	2,264	6.03%	35,269	93.97%
	Linear Crack	39,591	2,978	7.52%	36,613	92.48%
Route 2	Crack Distress	20,122	1,547	7.69%	18,575	92.31%
	Interconnected Crack	20,217	1,522	7.53%	18,695	92.47%
	Linear Crack	21,041	1,703	8.09%	19,338	91.91%
Route 3	Crack Distress	12,106	208	1.72%	11,898	98.28%
	Interconnected Crack	13,001	191	1.47%	12,810	98.53%
	Linear Crack	12,469	265	2.13%	12,204	97.87%
Sum	Crack Distress	68,105	4,129	6.06%	63,976	93.94%
	Interconnected Crack	70,751	3,977	5.62%	66,774	94.38%
	Linear Crack	73,101	4,946	6.77%	68,155	93.23%

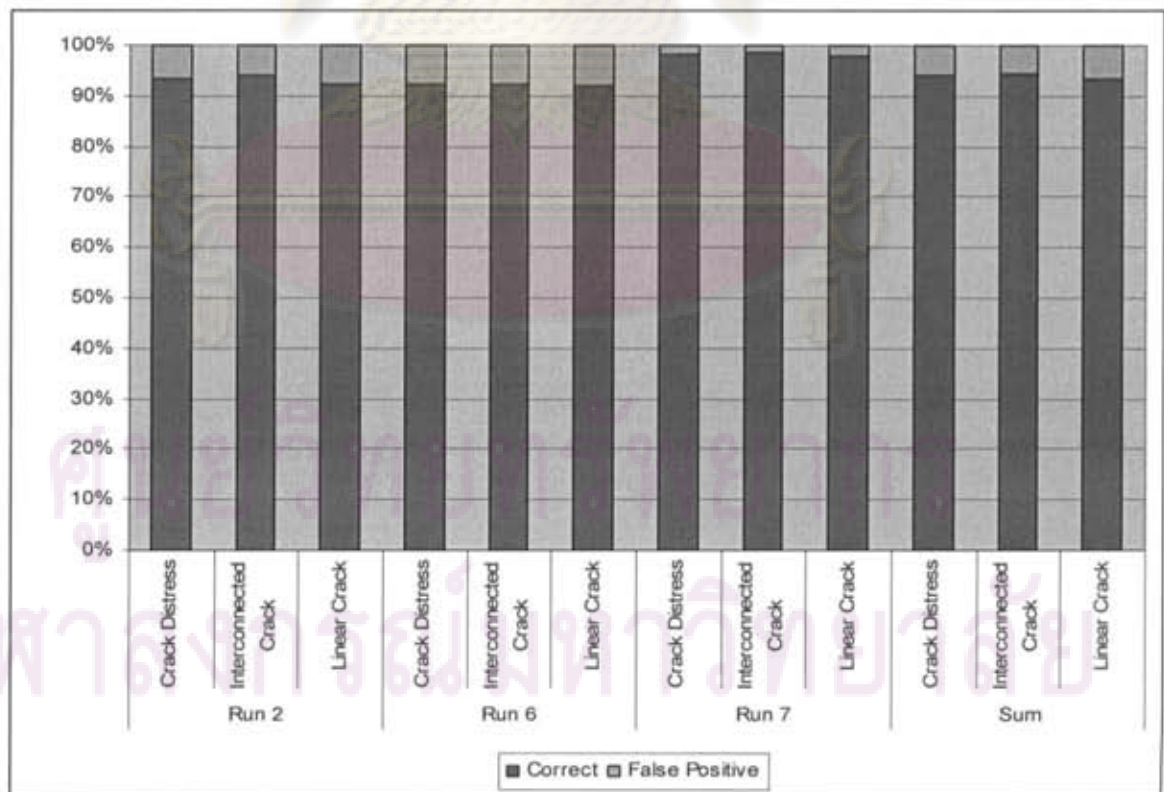


Figure A.1 False Positive in Mixed-Characteristic Input Images

Table A.2 False Negative in Mixed-Characteristic Input Images

Route	Type Image	Clean Images				
		Total	Crack Found (False Positive)		Crack Not Found (Correct)	
Route 1	Crack Distress	5488	3157	57.53%	2331	42.47%
	Interconnected Crack	3832	1596	41.65%	2236	58.35%
	Linear Crack	1774	1203	67.81%	571	32.19%
Route 2	Crack Distress	1031	946	91.76%	85	8.24%
	Interconnected Crack	936	661	70.62%	275	29.38%
	Linear Crack	112	77	68.75%	35	31.25%
Route 3	Crack Distress	1302	848	65.13%	454	34.87%
	Interconnected Crack	407	170	41.77%	237	58.23%
	Linear Crack	939	534	56.87%	405	43.13%
Sum	Crack Distress	7821	4951	63.30%	2870	36.70%
	Interconnected Crack	5175	2427	46.90%	2748	53.10%
	Linear Crack	2825	1814	64.21%	1011	35.79%

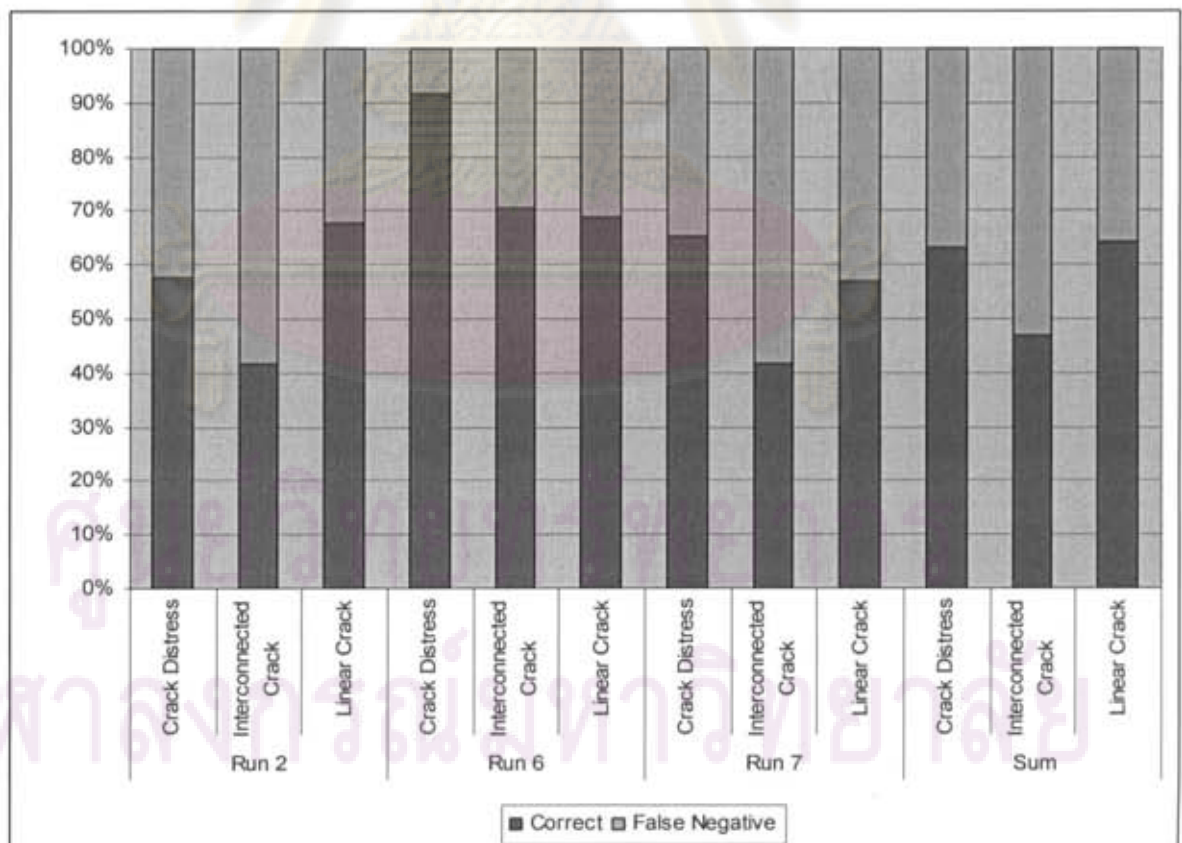


Figure A.2 False Negative in Mixed-Characteristic Input Images

Table A.3 Investigation of False Negative in Mixed-Characteristic Input Images

Excluding out-of-scope Images

Route	Interconnected Crack	Linear Crack	Human Fault
Route 1	145	60	16
Route 2	57	33	7
Route 3	229	280	78
Sum	431	373	101

Table A.4 Investigation of False Negative in Mixed-Characteristic Input Images

Excluding out-of-scope Images and Human Fault

Route	Crack Type	Classification Fault	Gradient Crack	Thin Crack	Crack Cell Found but Cannot be Grouped as Crack
Route 1	Interconnected	90	40	8	7
	Linear	8	10	24	2
Route 2	Interconnected	13	16	20	7
	Linear	3	19	4	1
Route 3	Interconnected	114	45	45	25
	Linear	10	127	53	12
Sum		238	257	154	54

ศูนย์วิทยทรัพยากร  
จุฬาลงกรณ์มหาวิทยาลัย



## Appendix B

### Publication

"Crack Detection on Asphalt Surface Image Using Enhanced Grid Cell Analysis" was presented in 4th IEEE International Symposium on Electronic Design, Test & Applications (DELTA 2008). The symposium was held at Hong Kong University of Science and Technology, Hong Kong, on January 23-25, 2008. This paper was published in the proceeding of DELTA 2008, pages 49-54.



ศูนย์วิทยทรัพยากร  
จุฬาลงกรณ์มหาวิทยาลัย

## Crack Detection on Asphalt Surface Image Using Enhanced Grid Cell Analysis

Siwaporn Sorncharean and Suebskul Phiphobmongkol  
 Department of Computer Engineering, Chulalongkorn University  
 Pathumwan, Bangkok, 10330, Thailand  
 Siwaporn.So@student.chula.ac.th, Suebskul.p@chula.ac.th

### Abstract

*This paper presents image processing techniques based on grid cell analysis for crack detection on non-uniform illumination and strong texture images. The techniques are Grid Cell Analysis Chain and Cracked Cell Verification. Grid Cell Analysis Chain helps eliminate false detection of shadow border on an image as being a cracked line. Cracked Cell Verification helps eliminate false detection when a grid cell has some image noise or strong texture but does not really contain part of a cracked line. Good accuracy in finding cracked lines on a pavement image with non-uniform illumination and strong texture can be achieved with 13% and 21% of false positive and false negative respectively.*

### 1. Introduction

Highway management system is typically used for estimating the budget and for making maintenance plans. Like all systems, the input of correct data is essential. Submitting incorrect raw data can envisage circumstances that would cause grave financial distress to local, regional, and national governments.

When looking at the area of pavement distress, visual inspection by human inspectors is time consuming, requires too many professional inspectors, and is financially restrictive. Moreover, distress classification and measurement are subjective. Two inspectors may give different results of distress information even if they are looking at the same thing.

To solve these problems, automatic crack monitoring systems were applied. An automatic system [1] can be separated into two phases. In the first phase, the system collected road surface images using a camera installed on a survey vehicle. In the second phase, an automatic processing of collected

images was performed to locate and measure distress.

A major problem of the automatic system is the accuracy of distress information from automatic image processing phase. This problem is caused by the quality of collected images. Most systems up until now use area scan cameras which were installed on survey vehicles. The area scan camera captures an image of a certain size and resolution. The bigger the area covered, the more tendencies to have non-uniform illumination on an image.

To improve the quality of images, a research [2] recommended the use of line scan cameras with artificial light to give uniform illumination and to remove shadow in the images. Because one strip or width of the pixel was captured with enough light, the captured images were of good quality with uniform light and the cracked lines were obvious to be noticed.

Even though, line scan seems to give better quality of road surface images, many old systems still use area scan cameras. Also, the need for better crack detection algorithm for area scan images can come from the need to re-extract cracking information of archived images. For example, studying about how cracks grow as time passed by needs accurate cracking information from archived images. Therefore, suitable crack detection algorithm for area scan images is still necessary.

Many crack detection techniques have been proposed. For example, an inspection system with image processing algorithm for detecting cracks in a tunnel [3] applied Sobel and Laplacian operators to find crack edges. It also applied a graph search method to find a cracked line using two points in an image. However, this system was semi-automatic, which needs the starting point and the ending point of each crack indicated by user. In addition, this system was applied to the indoor structure, e.g. a road tunnel wall, or a subway tunnel wall. The characteristics of these walls were different from the characteristics of an asphalt surface.

Artificial Intelligence is another technique used to find cracked area. For instance, a method using artificial living system [4] was proposed to remove



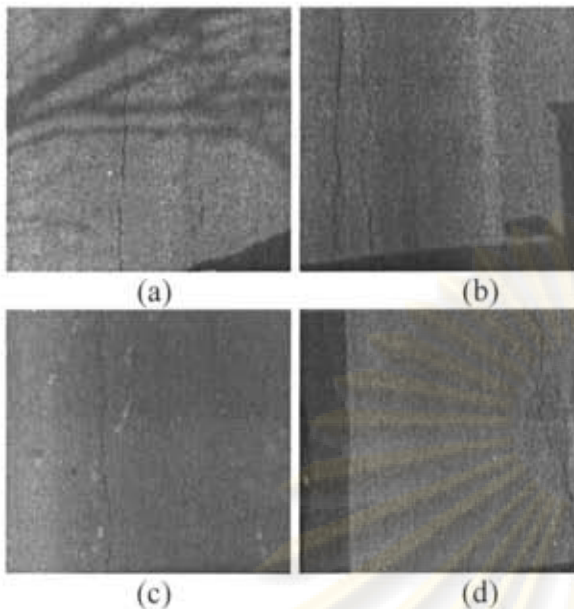


**Figure 1.** Example Images with Illumination and Texture Problems

noise, oil stains, and dark spots. A study by Tomikawa, was based on the basics of appropriate template matching controlled by a genetic algorithm [5]. Neural network was used to identify cracks by analyzing images extracted from video sequences [6]. Most artificial Intelligence techniques give good results. However, those techniques need a large training data set which takes a lot of time to construct and the training time is very long.

In 2006, a wavelet-based image processing method was also applied in automation for crack detection on pavement surface image [7]. The idea of using wavelet-based was to define the most adapted mother wavelet function for various pavement textures. In the same year, Huang and Xu [8] presented an image processing algorithm for inspection of pavement cracking. Their research consisted of three main steps. The first step was called grid cell analysis (GCA). In this step, the pixels that were chosen as cracked cells were regarded as a crack seed. The second step verified a crack seed by using the contrast of the crack seed to its neighbours. The last step was crack cluster connection. This step connected individual seeds into seed clusters for crack identification in a later phase. Nevertheless, this algorithm is suitable for images from

line scan camera with uniform artificial light. In addition, this solution needs preset thresholds that are not suitable for non-uniform illumination images.

This paper proposed an algorithm for crack detection on asphalt surface images. The method is based on a grid cell analysis which divides an image into grid cells and extracts cracking information from each cell. This method has strong effect on non-

uniform illumination images and strong texture images

## 2. Crack Detection Difficulties

There are two major difficulties in a crack detection process. The first difficulty is due to a survey with an area scan camera in an open environment where the light condition is a considerable problem. There is a lot of unavoidable shadow and shading in the images. Figure 1(a) shows unavoidable shadow from surrounding, e.g. tree branches. Figure 1(b) shows shadow from the survey vehicle. Moreover, an area scan camera cannot give uniform illumination images, even if there is no shadow. The image with illumination problem is shown in Figure 1(c)

The second important difficulty is due to the pavement texture. From the hypothesis, a crack is a narrow strip of pixels whose intensity is perceptible darker than the surrounding background. However, strong texture makes cracks and background blend together, which is shown in Figure 1(d). Gradient crack, a cracked line with low contrast to the neighbouring background, is another example. It is easy for human to define gradient cracked area, but difficult for image processing.

## 3. Grid Cell Analysis (GCA)

In GCA presented by Huang and Xu [8], a pavement image was divided into grid cells of 8x8 pixels and each grid cell was classified as a cracked or a non-cracked cell using the grayscale information of the border pixels as shown in Figure 2.

The first column in Figure 2 shows the original

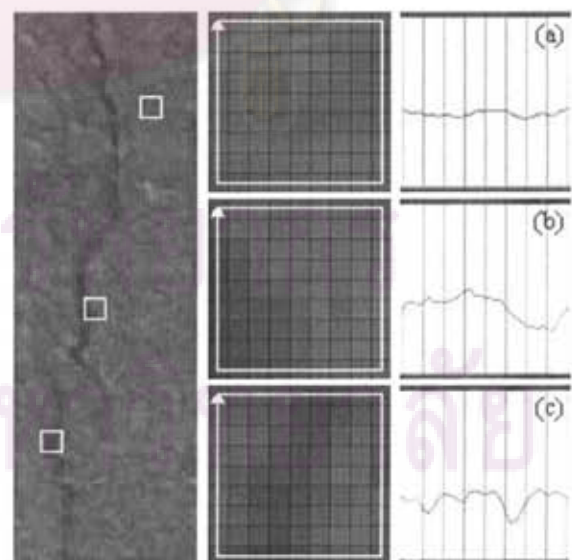


**Figure 2.** Grid Cell Attributes in Pavement Image

image, the second column shows the enlarged grid cells and the last column shows the border brightness profiles where two strips represent one side of the grid cell.

A cracked cell is identified by comparing its features from cracking information to preset thresholds. Cracking information includes the length, the width, and the contrast of a dark object. It also includes mean brightness, minimum brightness, and the presence of a dark strip within the cell, which is the valley in the border brightness profile. When a cell does not contain a crack, its border profile shows no apparent valleys as shown in Figure 2(a). In Figure 2(c), the border profile shows two sharp valleys, indicating the crossing points of a crack on the border. Figure 2(b) shows only one significant valley in the border grayscale, so the cell may have an edge crack. The result of the grid cell analysis is a seed point which is the darkest spot in the cell.

## 4. System Configuration

### 4.1. Hardware

The survey system used in this paper consisted of an area scan camera with a resolution of 1024 x 960 pixels. The camera covered approximately 1.86 x 1.75 square meters with a ground resolution of 1.8 mm/pixel. The image processing ran on an Intel Centrino Duo 2.16 GHz computer with 1GB RAM.

### 4.2. Grid Cell Size

Grid cell size selection is important for grid cell analysis. It strongly depends on crack size in terms of pixel width. Bigger or smaller grid cell size may not show enough information of cracking. Figure 3 shows grid cells above the same cracked area in an image. The grid cells are shown in three different sizes with their corresponding border brightness profiles. When the grid cell is too small, as shown in Figure 3(a), there is no noticeable valley in the profile. Figure 3(c) shows the cell whose size is too

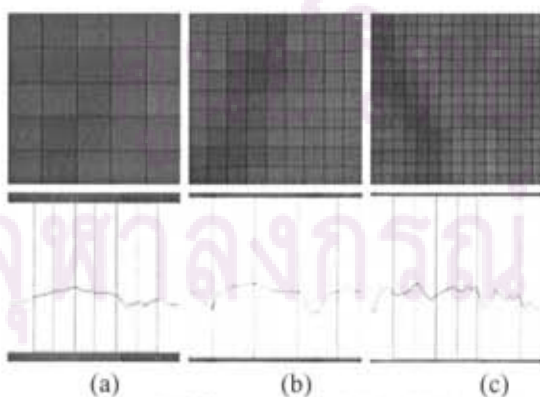


Figure 3. Difference Grid Cell Size with its Border Brightness Profile

big. It gives many valleys, thus the crossing points of a crack on the border are indistinct. The proper profile should have two clear-shape valleys as shown in Figure 3(b).

The grid cell size is also related to the crack width or the width of the dark strip. The proper grid cell size should be approximately triple of crack width. For example, five-millimetre crack appears in an image from this system as 3 dark pixels in strip width. So the grid cell size should be 9 pixels in width and height. In this paper, a grid cell size of 9x9 was used.

## 5. The Proposed Approach

The proposed approach can be separated into three phases. The first phase is the pre-processing phase for improving the original image. The second phase, called the Grid Cell Analysis Chain, handles shadow problems. The last phase is the Cracked Cell Verification, which guarantees the cracked cells. The algorithm of this approach is shown in Figure 4.

### 5.1. Pre-processing Phase

Generally, the asphalt surface images from a survey camera have faded and disconnected cracks, and too many dark and white spots. This situation perplexes the algorithm to find the dark strip objects. In order to enhance the cracks, i.e. to put them together and to remove noise, morphological operations in grayscale images are applied to improve the original image. This technique connects the dark pixels together, and removes isolated dark spots.

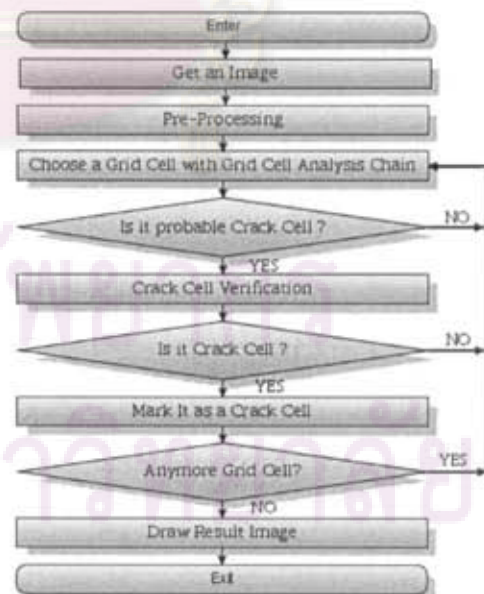


Figure 4. Enhanced Grid Cell Analysis Flow Chart



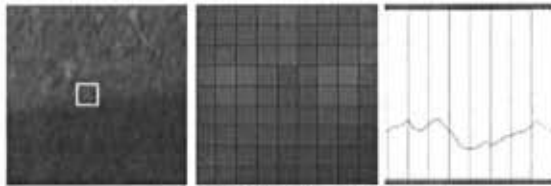


Figure 5. Grid Cell Attribute above Edge of Shadow Area

### 5.2. Grid Cell Analysis Chain

From GCA, the pavement image is divided into grid cells which are classified as cracked or non-cracked cells. In contrast to GCA which needs preset thresholds, Grid Cell Analysis Chain uses the border brightness profiles with hill climbing technique to find the valleys in order to handle the non-uniform illumination images.

In many cases, a profile with one significant valley is not always a cracked cell when implementing with shadow and shading images. As shown in Figure 5, the grid cell covering the edge of a shadow area gives a profile that looks like an edge cracked cell in Figure 2(b). To avoid this problem, instead of using two cases of profiles to indicate a crack cell, the profile which might be the crack cell must show only two considerable valleys, otherwise it is likely to be non-crack cell.

However, the above method would eliminate the cells that have edge crack. Double checking on images is necessarily applied. After divided into grid cells, the original image is divided again in overlapping area as given in Figure 6. This method can extract the cracked area and keep it away from the edge of shadow.

Figure 6 shows an overlapping area over different surfaces. Figure 6(a) is an image over a cracked area while Figure 6(b) is an image over a shadow area. Both profiles in the left side of Figure 6 look quite similar with one significant valley, which means they are non-crack cells. Consequently, cracked area in Figure 6(a) is ignored. After shifting the cell, the right profile in Figure 6(a) shows two significant valleys while the right profile in Figure 6(b) shows only one. That is, the cracked area in Figure 6(a) is extracted, whereas the shadow area is not.

### 5.3. Cracked Cell Verification

Strong texture is another problem that reduces the accuracy. Figure 7 shows a non-cracked cell with a profile which is similar to a cracked profile.

From the basic concept, a border profile which shows two sharp valleys indicates that there are two

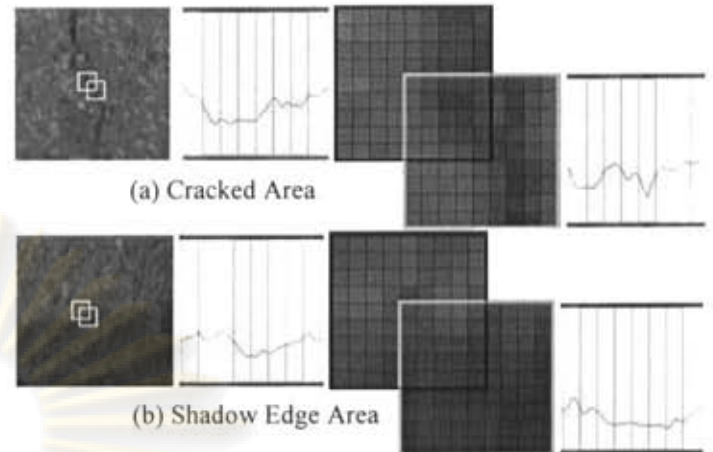


Figure 6. Grid Cell Attributes with Overlapping Grid Cells

crossing points of a crack on the border, but it does not guarantee that a cracked line is in the cell. To ensure the cracked cell, it would be verified. If there are dark pixels arranging in a line between two valleys, the cell is verified as a cracked cell.

The distance  $d$  between dark point  $p(x, y)$  and the imaginary-line between point  $q(x_1, y_1)$  and point  $q(x_2, y_2)$  is shown below.

$$d = \sqrt{(x - x_c)^2 + (y - y_c)^2}$$

Where

$$x_c = \frac{m^2 x_1 - m y_1 + m y_2 + x_2}{m + 1}$$

$$y_c = m x_c - m x_1 + y_1$$

$$m = \frac{y_2 - y_1}{x_2 - x_1}$$

To verify the cracked cell, all distances between each dark pixel to the imaginary-line must be within the crack size. Figure 8 shows arrangements of dark pixels and the imaginary-line. The dark pixels in Figure 8(a) are not adjacent to the imaginary-line whereas the dark pixels arrangement in Figure 8(b) closely resemble to the line.

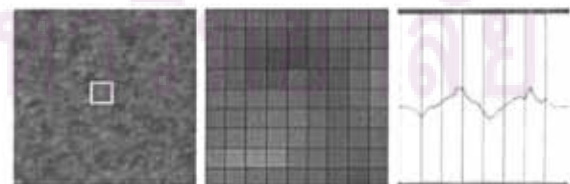


Figure 7. Grid Cell Attribute with Strong Texture

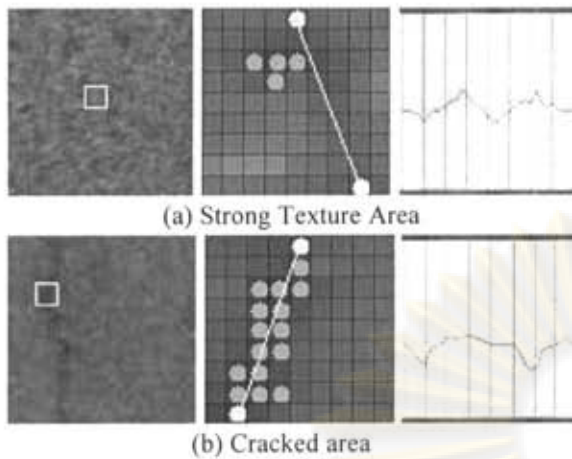


Figure 8. Grid Cell Attributes with Crack Arrangement

## 6. Experimental Results

Applying former GCA to sample images, the result images are shown in Figure 4.6(a). There are too many noises appearing in the result images from strong texture and shadow problems. After applying the first technique, Grid Cell Analysis Chain, to the sample images, the noises from the shadow are disappeared while the noises from strong texture are still in the result images as shown in Figure 4.6(b). Finally, both techniques are applied to the sample images. From the result images shown in Figure 4.6(c), this approach can extract cracks from the sample images and result in less noise.

Compared to another algorithm, the approach in this paper is more insensible to light condition. Figure 10 column (a) shows the result images implemented with this approach, and column (b) shows the result images implemented with the Huang and Xu algorithm [8]. The sample images have different brightness and some have low contrast. Both algorithms were applied with the same parameter to those images. The results which applied by the proposed algorithm were satisfactory, while the other gives the best result in the first image of Figure 10. In the other images, it gives unsatisfied results.

Moreover, the proposed approach has been applied to 3,676 asphalt road images from different environment with strong texture and shadow environment in order to measure the accuracy. The input images also contain other types of distress, i.e. ravelling surface and poor patching area which give too-strong-texture images. Furthermore, the input images include poor illumination conditions which give low contrast images. Input images are classified into two categories by human inspectors, cracked and non-cracked images. This experiment used grid cell size of 9x9 to find crack size of 5 mm. The

Table 1: Testing Result on Asphalt Road Images

	Total	True	False
Non-Cracked Images	2,329	2,037 87%	292 13%
Cracked Images	1,347	1,061 79%	286 21%

results are shown in table 1. This approach gives 13% of false positive, 21% of false negative in the summary results.

## 7. Conclusion

This paper introduces image processing techniques for crack detection in asphalt surface images. This paper is based on Grid Cell Analysis (GCA) technique to classify cracked cells. The approach consists of three phases. The first phase is the pre-processing phase which improves original images. The second phase is the Grid Cell Analysis Chain which solves shadow and shading problems. This phase decreases the number of conditions for indicating cracked cell in order to reduce noise. It

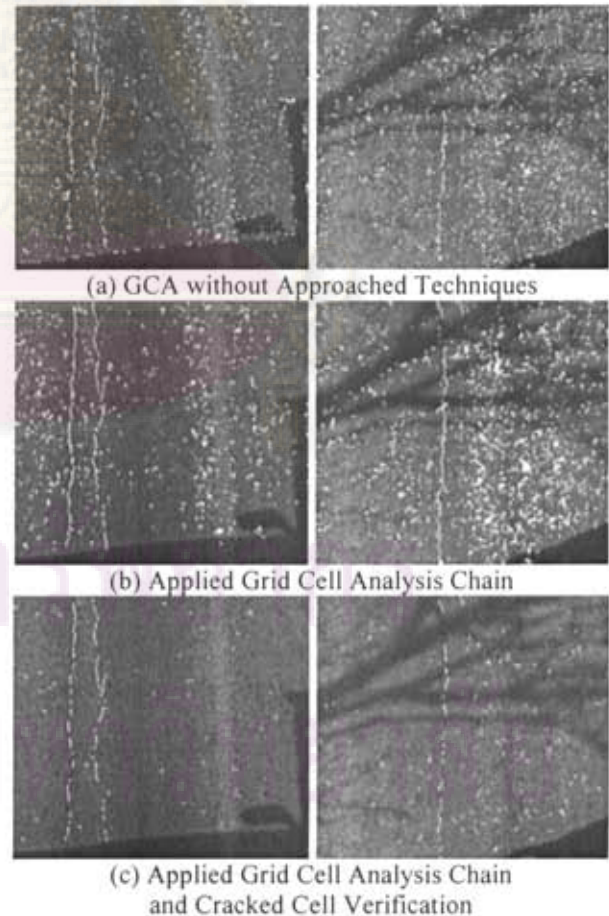
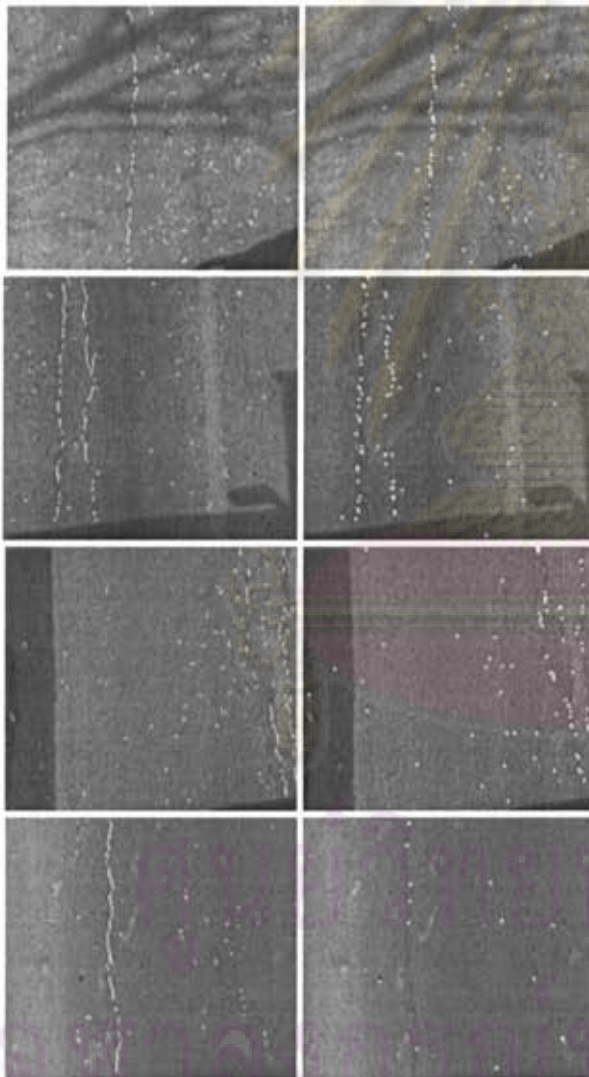


Figure 9. Examples of Result Images



also increases the working areas on the image by dividing the image in overlapping area. The third phase is the Cracked Cell Verification which uses the assumption that all the cracked cells should have crack pixel arrangement closed to the imaginary-line.

The measurement results were satisfactory with 13% and 21% of false positive and false negative respectively. Thus, several images, in the case of which the system shows no distress, can be skipped. Human inspectors can focus only on images with distress results. Therefore, this algorithm helps reduce human work in a survey, and gives more accurate and reliable data to highway management system.



(a) Proposed Approach (b) Previous Approach

**Figure 10.** Experimental Result Images Compared with Previous Algorithm with Same Variable Values

## 8. Acknowledgements

We wish to acknowledge the financial support provided by Commission on Higher Education, Ministry of Education, Kingdom of Thailand, and would like to thank Associate Professor Dr. Wisanu Subsompon, and members at Transportation Institute, Chulalongkorn University, Thailand, for advices and helps in the project.

## 9. References

- [1] J. Pynn, A. Wright, and R. Lodge, "Automatic identification of cracks in road surfaces", *Seventh International Conference on Image Processing and Its Applications, Manchester, UK*, vol. 2, 1999, pp 671-675.
- [2] I. Sokolic, "Criteria to Evaluate the Quality of Pavement Camera Systems in Automated", Civil and Environmental Engineering, University of South Florida, 2004.
- [3] S.-N. Yu, J.-H. Janga, and C.-S. Han, "Auto inspection system using a mobile robot for detecting concrete cracks in a tunnel", *Automation in Construction*, vol. 16, 2007, pp 255-261.
- [4] H. G. Zhang and Q. Wang, "Use of Artificial Living System for Pavement Distress Survey", *Industrial Electronics Society 2004, 30th Annual Conference of IEEE, IEEE Computer Society*, vol. 3, 2004, pp 2486-2490.
- [5] T. Tomikawa, "A study of road crack detection by the meta-genetic algorithm", *AFRICON, IEEE, Cape Town, South Africa*, vol. 1, 1999, pp 543-548.
- [6] D. Meignen, M. Bernadet, and H. Briand, "One Application of Neural Networks for Detection of Defects Using Video Data Bases: Identification of Road Distresses", *Proceedings of the 8th International Workshop on Database and Expert Systems Applications, IEEE Computer Society*, 1997, pp 459-464.
- [7] P. Subirats, J. Dumoulin, V. Legeay, and D. Barba, "Automation of Pavement Surface Crack Detection using the Continuous Wavelet Transform", *2006 IEEE International Conference on Image Processing*, 2006, pp 3037-3040.
- [8] B. Xu, Y. Huang, "Automatic Inspection of Pavement Cracking Distress", *Journal of Electronic Imaging*, vol. 15, 2006.

## Biography

Siwaporn Sorncharean was born in Bangkok, Thailand, on January 26, 1984. She got a Bachelor degree in Computer Engineering from King Mongkut's University of Technology Thonburi in 2006. She is currently pursuing the Master degree in Computer Engineering at Chulalongkorn University.



ศูนย์วิทยทรัพยากร  
จุฬาลงกรณ์มหาวิทยาลัย